Multi-parameter dynamical diagnostics for upper tropospheric and lower stratospheric studies

Millán, L. F., Manney, G. L., Boenisch, H., Hegglin, M. I. ORCID: https://orcid.org/0000-0003-2820-9044, Hoor, P., Kunkel, D., Leblanc, T., Petropavloskikh, I., Walker, K., Wargan, K. and Zahn, A. (2023) Multi-parameter dynamical diagnostics for upper tropospheric and lower stratospheric studies. Atmospheric Measurement Techniques, 16 (11). pp. 2957-2988. ISSN 1867-8548 doi: https://doi.org/10.5194/amt-16-2957-2023 Available at https://centaur.reading.ac.uk/120150/

Atmos. Meas. Tech., 16, 2957–2988, 2023
https://doi.org/10.5194/amt-16-2957-2023

Atmospheric Measurement Techniques
Open Access
EGU

Multi-parameter dynamical diagnostics for upper tropospheric and lower stratospheric studies

Luis F. Millán[1], Gloria L. Manney[2,3], Harald Boenisch[4], Michaela I. Hegglin[5,6,7], Peter Hoor[8], Daniel Kunkel[8], Thierry Leblanc[9], Irina Petropavlovskikh[10], Kaley Walker[11], Krzysztof Wargan[12,13], and Andreas Zahn[4]

[1]Jet Propulsion Laboratory, California Institute of Technology, Pasadena, California, USA
[2]NorthWest Research Associates, Socorro, New Mexico, USA
[3]Department of Physics, New Mexico Institute of Mining and Technology, Socorro, New Mexico, USA
[4]Karlsruhe Institute of Technology, Institute of Meteorology and Climate Research, Karlsruhe, Germany
[5]Institute of Energy and Climate Research, Stratosphere (IEK-7), Forschungszentrum Jülich, Jülich, Germany
[6]Department of Meteorology, University of Reading, Reading, UK
[7]Department of Atmospheric Physics, University of Wuppertal, Wuppertal, Germany
[8]Institute for Atmospheric Physics, University of Mainz, Mainz, Germany
[9]Jet Propulsion Laboratory, California Institute of Technology, Wrightwood, California, USA
[10]Cooperative Institute for Research in Environmental Sciences, National Ocean and Atmospheric Administration, Boulder, Colorado, USA
[11]Department of Physics, University of Toronto, Toronto, Canada
[12]Science Systems and Applications Inc., Lanham, Maryland, USA
[13]Global Modeling and Assimilation Office, NASA Goddard Space Flight Center, Greenbelt, Maryland, USA

Correspondence: Luis F. Millán (lmillan@jpl.nasa.gov)

Received: 4 February 2023 – Discussion started: 6 March 2023
Revised: 9 May 2023 – Accepted: 11 May 2023 – Published: 15 June 2023

Abstract. Ozone trend estimates have shown large uncertainties in the upper troposphere–lower stratosphere (UTLS) region despite multi-decadal observations available from ground-based, balloon, aircraft, and satellite platforms. These uncertainties arise from large natural variability driven by dynamics (reflected in tropopause and jet variations) as well as the strength in constituent transport and mixing. Additionally, despite all the community efforts there is still a lack of representative high-quality global UTLS measurements to capture this variability.

The Stratosphere-troposphere Processes And their Role in Climate (SPARC) Observed Composition Trends and Variability in the UTLS (OCTAV-UTLS) activity aims to reduce uncertainties in UTLS composition trend estimates by accounting for this dynamically induced variability. In this paper, we describe the production of dynamical diagnostics using meteorological information from reanalysis fields that facilitate mapping observations from several platforms into numerous geophysically based coordinates (including tropopause and upper tropospheric jet relative coordinates). Suitable coordinates should increase the homogeneity of the air masses analyzed together, thus reducing the uncertainty caused by spatiotemporal sampling biases in the quantification of UTLS composition trends. This approach thus provides a framework for comparing measurements with diverse sampling patterns and leverages the meteorological context to derive maximum information on UTLS composition and trends and its relationships to dynamical variability.

The dynamical diagnostics presented here are the first comprehensive set describing the meteorological context for multi-decadal observations by ozonesondes, lidar, aircraft, and satellite measurements in order to study the impact of dynamical processes on observed UTLS trends by different sensors on different platforms. Examples using these diagnostics to map multi-platform datasets into different geophysically based coordinate systems are provided. The diagnostics presented can also be applied to analysis of greenhouse

gases other than ozone that are relevant to surface climate and UTLS chemistry.

1 Introduction

Despite decades of spaceborne, airborne, balloon-borne, and ground-based measurements, confidence in upper troposphere–lower stratosphere (UTLS) long-term ozone trends remains low (e.g., Harris et al., 2015; Steinbrecht et al., 2017; Petropavlovskikh et al., 2019; Szeląg et al., 2020; Godin-Beekmann et al., 2022). For example, Ball et al. (2018), using multiple satellite measurements, reported that ozone in the lower stratosphere between 60° S and 60° N showed a statistically significant decline. Wargan et al. (2018) suggest that these downward trends were driven by enhanced isentropic transport between the tropical (20° S–20° N) and extratropical lower stratosphere, while Orbe et al. (2020) suggest that in the midlatitudes in the Northern Hemisphere these downward trends were mostly related to large-scale advection. Further, as discussed by Chipperfield et al. (2018), expanding the satellite time series from 1998–2016 to 1998–2017 changed the trend interpretation from one of decline to one of large dynamical variability, in agreement with the study by Stone et al. (2018). Ball et al. (2019) argued that while the inclusion of additional years (2017 and 2018) confounds the ozone trends in the Southern Hemisphere lower stratosphere, the trends in the Northern Hemisphere still showed a statistically significant decline. Lastly, Thompson et al. (2021), Bognar et al. (2022), and Match and Gerber (2022) showed that most of the downward trends in the tropics are attributable to increases in tropopause altitude due to tropospheric warming.

Some of the reasons for this low confidence in the UTLS trends are as follows:

- The Brewer–Dobson circulation (BDC) and transport from the troposphere into the stratosphere and vice versa which influence the structure and composition of the UTLS (e.g., Gettelman et al., 2011) exhibit large dynamical variability, rendering statistical evaluations of ozone trends difficult and sensitive to the time period (start and end points) chosen. Many variations in UTLS ozone are associated with geographic and temporal variations in the tropopause and upper tropospheric jet streams (Pan et al., 2009; Manney et al., 2011; Schwartz et al., 2015; Albers et al., 2018; Olsen et al., 2019, and references therein).

- Long-term trends in these dynamical features (such as trends in the positions of the jets, the tropopause, and systematic changes in the BDC) confound the long-term trends in ozone due to chemistry. For example, global tropopause altitudes and the frequency of double tropopauses increased substantially between 1981 and 2015 (e.g., Xian and Homeyer, 2019). Subtropical jet strength and position trends show large regional and seasonal variations, but jet altitudes have typically increased (consistent with reports of tropopause altitude increases related to climate change), while their velocities in general increased in winter and decreased in summer between 1980 and 2014 (e.g., Manney and Hegglin, 2018). The attribution of jet trends, particularly the polar (or "eddy-driven") jet, is an active research topic, with different studies arguing for either strengthening or weakening of the jets with climate change (e.g., Barnes and Screen, 2015; Francis, 2017; Manney and Hegglin, 2018).

- Available measurements cannot completely represent the global structure and variability of the UTLS, since the balloon-borne and ground-based measurements have limited geographical and temporal coverage. The aircraft measurements from regular passengers flights cover a limited altitude range (mostly one altitude level per flight, except during takeoff and landing) while research campaigns are limited to regional coverage and short time periods, and space-borne measurements have horizontal and vertical resolutions that are too coarse. For example, Millán et al. (2016), using sampled and raw model fields, showed that even dense satellite sampling patterns may have up to 10 % bias in the zonal mean representation of UTLS ozone.

Analyzing datasets in conventional coordinates (e.g., altitude or pressure/latitude grids using zonal means) does not account for local and regional variability impacting ozone gradients at the tropopause and the jets. It thus entangles the impact of dynamics on ozone with impacts of other processes (e.g., chemistry). To increase confidence in UTLS composition trends, the Observed Composition Trends and Variability in the UTLS (OCTAV-UTLS) Stratosphere-troposphere Processes And their Role in Climate (SPARC) activity (see http://www.octav-utls.net for more information, last access: 1 February 2023) was initiated in 2018. This activity aims to analyze multi-platform measurements in coordinate systems that account for the geophysical variability of the jets and tropopause.

The use of well-suited coordinates can increase consistency in locating the measurements with respect to dynamical barriers and thus more accurately represent tracer gradients, which in turn will increase the homogeneity of the air masses mapped within the bins in such coordinate systems. For example, Pan et al. (2004), Hoor et al. (2004), and Hegglin et al. (2006) have shown that using tropopause-related coordinates (i.e., altitude relative to the tropopause) greatly reduces the scatter around the tropopause, revealing a sharp gradient between tropospheric and stratospheric air masses; Manney et al. (2011) and Olsen et al. (2019) have similarly shown that jet-relative coordinates reduce scatter in the horizontal revealing sharp gradients across the UT jets.

To derive these dynamically based coordinates, a consistent characterization of the measurements using meteorological fields is required. In this paper we describe the generation of dynamical diagnostics for multi-platform ozone datasets. Apart from allowing mapping of the measurements into coordinates that should segregate measurements of ozone with similar characteristics, these dynamical diagnostics have already been used (among other examples) to study stratospheric and UTLS transport in several Arctic winters (e.g., Manney et al., 2009), to obtain a global view of the chemical characteristics of the extratropical tropopause transition region (Hegglin et al., 2009), to study the impact of double tropopauses on UTLS composition (Schwartz et al., 2015), to characterize biomass-burning plumes (Tereszchuk et al., 2011, 2013), to study UTLS transport and mixing timescales (Hoor et al., 2010), to study UTLS ozone variability (Thouret et al., 2006; Manney et al., 2011; Cohen et al., 2018; Olsen et al., 2019), to intercompare CO measurements in the tropopause region (Martínez-Alonso et al., 2014), to assess the reanalyses representation of ozone mini-holes (Millán and Manney, 2017), to characterize the composition of the Asian summer monsoon anticyclone (Santee et al., 2017), and to study cyclone-induced surface ozone and HDO depletion in the Arctic (Zhao et al., 2017).

The purpose of the present paper is twofold: first, it introduces the OCTAV-UTLS SPARC activity, and, second, it provides information and examples of the dynamical diagnostics to be used in future OCTAV-UTLS activity studies.

2 OCTAV-UTLS

As already mentioned, the OCTAV-UTLS SPARC activity aims to reduce uncertainties in UTLS composition trend estimates by accounting for dynamically induced variability (Kunkel et al., 2018; Hoor et al., 2019; Leblanc et al., 2020). The distribution of tracers (not only ozone) in the UTLS shows large spatial and temporal variability, caused by competing transport, chemical, and mixing processes near the tropopause; variations in the tropopause itself; and the position and variations of the jets (i.e., Hegglin et al., 2009; Manney et al., 2011). This strongly affects quantitative estimates of the impact of radiatively active substances, including ozone and water vapor, on surface temperatures (e.g., Forster and Shine, 1997; Riese et al., 2012) and complicates the diagnosis of dynamical and transport processes such as stratosphere–troposphere exchange (e.g., Gettelman et al., 2011). The community thus faces the challenge of optimally exploiting the vast existing portfolio of observations to better understand the physical composition of the UTLS.

Achieving OCTAV-UTLS goals requires a detailed characterization of existing measurements (from aircraft, ground-based, balloon, and satellite platforms) in the UTLS, including understanding how their quality and sampling characteristics (spatial and temporal coverage, resolution) affect the representativeness of these observations. Paramount to this effort is to develop and apply common dynamical diagnostics (described in this paper) to compare UTLS observations using a variety of geophysically based coordinate systems (e.g., equivalent latitude, relative to the tropopause, or relative to the jets) derived from meteorological information from reanalysis datasets. This approach provides a framework for comparing and eventually combining measurements with diverse sampling patterns and thus leverages the meteorological context to derive maximum information on UTLS composition and its relationships to dynamical variability.

Ultimately, taking into account the trends in the tropopause or jet locations will lead to more accurate and comprehensive trace species trend estimates in the UTLS. Thus, after the comparison of measurements with different sampling characteristics, OCTAV-UTLS will facilitate studying long-term trends in chemical species from the various observational platforms.

3 Datasets

Within OCTAV-UTLS, ozonesonde, lidar, aircraft, and satellite datasets will be used. Ozonesondes are in situ sensors normally flown attached to a balloon and interfaced with meteorological radiosondes (Komhyr, 1986; Komhyr et al., 1995). Recent ozonesondes are equipped with a GPS receiver. In short, the ozonesonde measures the current generated by the reaction of atmospheric ozone with a solution of potassium iodide, which is proportional to the ozone concentration.

The ozonesonde data used here were taken from the National Oceanic and Atmospheric Administration (NOAA) Global Monitoring Laboratory (GML) open-access archive. In the troposphere, typical 1σ uncertainties are around $\pm 5\,\%$ at midlatitudes and up to $\pm 20\,\%$ in the tropics; lower stratospheric uncertainties are around $\pm 4\,\%$–$6\,\%$ (e.g., Smit et al., 2007; Sterling et al., 2018; Tarasick et al., 2021). Their vertical resolution depends on the weight of the package, balloon size, weather conditions, and the sampling rate. Analog ozonesondes were able to sample approximately every 60 s, and digital models can sample up to every second (Sterling et al., 2018), resulting in a vertical resolution varying from approximately 300 to 5 m. Ozonesondes used in OCTAV-UTLS have been gridded to 250 m (for analog sondes) or 100 m (for digital sondes) to reduce computing power when calculating the dynamical diagnostics. In principle, ozonesonde records provide long-term UTLS ozone measurements under all weather conditions, that is, not biased toward clear-sky conditions. Table 1 lists the ozonesondes particulars.

Lidar (an acronym for light detection and ranging) is a laser remote sensing technique commonly used to measure atmospheric composition from the ground, aircraft, and occasionally space. One or more laser beams are emitted into

Table 1. Details of ozonesondes **(a)** and lidar **(b)** datasets processed and their primary characteristics.

Code	Name	Latitude	Longitude	Range	Time span
(a)					
SPO	South Pole, Antarctica	−89.98	−24.8	0–30 km[a]	1967–1971, 1986–
SUV	Suva, Fiji	−18.00	178.0	0–30 km	1997–
SMO	Tutuila, American Samoa	−14.24	−170.56	0–30 km	1986–1990, 1995–
HIH	Hilo, Hawaii, USA	19.72	−155.05	0–30 km	1982–
HVA	Huntsville, Alabama, USA	34.720	−86.64	0–30 km	1999–
BLD	Boulder, Colorado, USA	39.99	−105.26	0–30 km	1967–1971, 1979–
THD	Trinidad Head, California, USA	41.05	−124.15	0–30 km	1997–
SUM	Summit, Greenland	72.60	−38.42	0–30 km	2005–2017
(b)					
TMF	Wrightwood, California, USA	34.4	−117.7	10–50 km	1989–
TMF[b]	Wrightwood, California, USA	34.4	−117.7	0–22 km	1999–
OHP	Haute Provence, France	43.94	5.71	10–50 km	1985–
OHP[c]	Haute Provence, France	43.94	5.71	0–22 km	1991–
HOH	Hohenpeissenberg, Germany	47.80	11.02	10–50 km	1987–
MLO	Mauna Loa, Hawaii, USA	19.54	−155.58	10–50 km	1993–
LAU	Lauder, New Zealand	−45.04	169.68	10–50 km	1994–

[a] For all ozonesondes, the highest altitude depends on the bursting point of the balloon. [b] There are two different lidars at TMF, a stratospheric system (measuring since 1989) and tropospheric one (measuring since 1999). [c] There are two different lidars at OHP, a stratospheric system (measuring since 1985) and tropospheric one (measuring since 1991).

the atmosphere, and a fraction of the emitted light is scattered back to the lidar instrument receiver by molecules and particles, where it is sampled as a function of time, i.e., distance traveled from the instrument. Tropospheric and stratospheric ozone can be measured using the differential absorption lidar (DIAL) technique, for which two laser beams of different wavelengths are emitted and absorbed differently by ozone along their atmospheric path. This difference in absorption is used to deduce ozone number density (Mégie et al., 1977). The typical vertical resolution of ozone DIAL measurements ranges from a few meters in the lower troposphere to a few kilometers in the upper stratosphere. Precision typically ranges from less than 1 % to over 10 % depending on the altitude and vertical resolution considered (Leblanc et al., 2016). Table 1 also lists the lidars currently available.

Because of their technical complexity and cost, the number of ozone DIAL instruments is limited to less than a dozen around the world, thus implying limited geographical coverage. However, lidars have the capability to measure continuously for many hours or even days without interruption (e.g., Godin-Beekmann et al., 2002; Leblanc et al., 2018), making the technique very well suited for a wide range of atmospheric studies ranging from long-term monitoring to physical processes in support of meteorology and air quality forecast and modeling (e.g., Ravetta et al., 2007; Steinbrecht et al., 2009; Cooper et al., 2010; Langford et al., 2018; Zerefos et al., 2018). The long-term stability of ground-based lidar instruments also makes them very suitable for validation of airborne or satellite-based measurements (e.g., Jiang et al., 2007; Gijsel et al., 2009; Hubert et al., 2016; Wang et al., 2020; Wing et al., 2020; Mettig et al., 2022). Due to their inherent measurement sampling characteristics, lidars' effective vertical and temporal resolutions can be optimized to specific applications, making the lidar technique very versatile in comparison to other observation platforms (e.g., Leblanc et al., 2012).

Aircraft in situ measurements are typically made using UV photometry and/or chemiluminescence detectors (CLDs). UV photometry is based on the strong UV ozone absorption; simply, the light intensity measured by a photometer and the concentration of ozone in the absorption chamber are described by the Beer–Lambert law. CLDs use either a gaseous, solid, or liquid reagent. The sensor measures the intensity of light emitted from a reaction product in an electronically excited state, which is proportional to the ozone concentration. In particular, we use measurements from the following field campaigns:

- In-service Aircraft for a Global Observing System (IAGOS) Civil Aircraft for the Regular Investigation of the atmosphere Based on an Instrument Container (CARIBIC) (Brenninkmeijer et al., 1999, 2007);
- Spurenstofftransport in der Tropopausenregion (SPURT; which means trace gas transport in the tropopause region) (Engel et al., 2006);
- Stratosphere-Troposphere Analyses of Regional Transport (START08) (Pan et al., 2010);

- Transport and Composition in the Upper Troposphere and Lower Stratosphere and Earth System Model Validation (TACTS/ESMVal) (Müller et al., 2016);
- Polar Stratosphere in a Changing Climate (POLSTRACC) campaign (Oelhaf et al., 2019), operated with two other projects, the GW-LCYCLE (Investigation of the Life cycle of gravity waves) and SALSA (Seasonality of Air mass transport and origin in the Lowermost Stratosphere), known together as the PGS mission;
- Wave-driven ISentropic Exchange (WISE) (Kunkel et al., 2019).

Typical random errors are smaller than 1 % for newer systems (current CARIBIC measurements; Zahn et al., 2012) but around 5 % for older aircraft measurements (e.g., SPURT; Hegglin et al., 2006).

Aircraft measurements from commercial flights (IAGOS), although they are essentially line measurements limited in time and space, provide a very detailed view of UTLS ozone due to their high temporal resolution, relatively low measurement error, and long time series. Their 10 to 12 km cruising altitude coincides with the UTLS in middle and high latitudes. Research aircraft missions (such as SPURT, START08, and WISE) are limited in regional and temporal coverage but cover a larger portion of the UTLS in the vertical and thus are better suited to process studies. Table 2 lists aircraft campaign particulars.

Satellite ozone measurements can be cataloged according to their measurement geometry, namely, nadir emission; nadir scattering; limb emission; limb scattering; and solar, lunar, or stellar occultation (more information in chap. 2 of Hegglin and Tegtmeier, 2017). In particular, here we use solar occultation and limb emission measurements. Limb-viewing instruments generally yield a higher vertical resolution and larger sensitivity than nadir-viewing instruments in the stratosphere.

The solar occultation technique uses measurements of sunlight through the Earth's atmosphere and calculates ratios between them and ones where no atmospheric attenuation was present (i.e., a measurement above the atmosphere). Hence, the solar occultation technique is a self-calibrated measurement. These measurements provide a very high signal-to-noise ratio (due to the brightness of the sun), allowing the detection of species with very low atmospheric concentrations. The main limitation of this technique is that the measurements can only be taken during sunrise or sunset, constraining the number of measurements to two per orbit. The solar occultation measurements used here are from the Atmospheric Chemistry Experiment Fourier Transform Spectrometer (ACE-FTS) and Stratospheric Aerosol and Gas Experiment III on the International Space Station (SAGEIII/ISS).

ACE-FTS was launched in 2003 on board the Canadian SCISAT spacecraft, and measurements started in February 2004. It retrieves temperature, pressure, and concentration for several dozen atmospheric trace gases from infrared measurements (Bernath et al., 2005). ACE-FTS focuses on high-latitude science, and thus almost 50 % of its occultations occur at latitudes at or poleward of 60°. The nominal vertical resolution of this dataset (as defined by the field-of-view) is about 3 km, but Hegglin et al. (2008) showed that ACE-FTS is capable of resolving the UTLS with high accuracy, suggesting a nominal vertical resolution of around 1 km, which is achieved thanks to oversampling. That is, measuring at vertical spacing finer than the instrument field-of-view of 3 km. Studies validating the ozone data include Dupuy et al. (2009) and Sheese et al. (2017, 2022), among others. We have used ACE-FTS version 4.1.

SAGEIII/ISS was launched and delivered to the ISS in 2017, and routine measurements started in June 2017. It measures UV, visible, and near-IR sunlight through the Earth's limb to retrieve ozone, water vapor, nitrogen dioxide, and aerosol concentrations. The vertical resolution of this dataset is about 1 km. SAGEIII/ISS ozone measurements were validated by McCormick et al. (2020), Wang et al. (2020), and Hegglin et al. (2021). Here we have used SAGEIII/ISS version 5.2.

The limb emission viewing technique uses observations of thermal emission, that is, the radiation emitted by the atmosphere along a line of sight, to infer atmospheric constituents. These techniques provide day and night retrievals with dense sampling throughout the orbit. Limb emission measurements from the Aura Microwave Limb Sounder (MLS) are used here. MLS was launched on board NASA's Aura satellite and measurements started in August 2004. It measures limb millimeter and submillimeter atmospheric thermal emission, from which temperature, trace gas concentrations, and cloud ice are retrieved (Waters et al., 2006). Aura MLS ozone has around 3 km resolution in the UTLS and stratosphere (Livesey et al., 2020), and the data have been extensively validated (e.g., Jiang et al., 2007; Froidevaux et al., 2008; Livesey et al., 2008; Hubert et al., 2016). Here we use MLS version 5 (Schwartz et al., 2020).

Satellite observations, despite the coarser vertical and horizontal resolution in comparison with the other datasets here discussed, provide a global picture of the UTLS and can help with linking measurements with limited geometrical coverage. Table 3 lists these ozone satellite measurement characteristics including typical precision in the UTLS.

Figure 1 shows the sampling locations of the ozonesondes, lidars, aircraft, and satellite instruments used in OCTAV-UTLS. These datasets differ greatly in geographical coverage, horizontal and vertical resolution, measurement frequency, and time period covered. To fully exploit these measurements, careful attention needs to be paid to understand how sampling differences between the instruments can affect their representation of the atmospheric state (e.g, Heg-

Table 2. Details of aircraft datasets processed and their primary characteristics.

Campaign	Region	Time span	Technique	References
CARIBIC-1	N. Hemisphere	1997–2002	UV photometry	Brenninkmeijer et al. (1999)
CARIBIC-2	N. Hemisphere	2005–2020	UV photometry	Brenninkmeijer et al. (2007)
SPURT	Europe	2001–2003	CLD and UV photometry	Engel et al. (2006)
START08	Continental USA	2008	CLD and UV photometry	Pan et al. (2010)
TACTS/ESMVAL	Europe and Africa	2012	CLD and UV photometry*	Müller et al. (2016)
PGS	Arctic	2015–2016	CLD and UV photometry*	Oelhaf et al. (2019)
WISE	Europe and N. Atlantic	2017	CLD and UV photometry*	Kunkel et al. (2019)

* These campaigns all used the FAIRO instrument (Zahn et al., 2012).

Table 3. Satellite instrument datasets processed and their primary characteristics.

Instruments	Time span	No. profiles per day	Vert. res.	Range	UTLS error	References
Aura MLS	2004–	∼ 3500	∼ 3 km	316–0.01 hPa	∼ 30 % (UT) >4 % (LS)	Waters et al. (2006) Livesey et al. (2020)
ACE-FTS	2004–	∼ 30	3–4 km	5–90 km	3 %	Bernath et al. (2005), Dupuy et al. (2009)
SAGEIII/ISS	2017–	∼ 30	∼ 0.5 km	5–60 km	3 %	Wang et al. (2020)

glin et al., 2008; Toohey et al., 2013; Lin et al., 2015; Millán et al., 2016; Miyazaki and Bowman, 2017; Millán et al., 2018; Chang et al., 2020).

The datasets used here are not meant to be an exhaustive list of all the ozone records available; many other records exist. For example, the rest of the Network for the Detection of Atmospheric Composition Change (NDACC) ozonesonde records (e.g., De Mazière et al., 2018), the ozonesondes included in the Southern Hemisphere ADditional OZonesondes (SHADOZ) (Witte et al., 2017; Thompson et al., 2017), the IAGOS-CORE (Petzold et al., 2015), or the limb scattering satellite sounders, the Optical Spectrograph and Infrared Imager System (OSIRIS) (Llewellyn et al., 2004) or the Ozone Mapping and Profiler Suite (OMPS) (Seftor et al., 2014). However, the records included in this study are meant to be representative of the currently available ozone datasets in terms of resolution as well as geographical sampling and with a focus on the extratropical UTLS, where tropopause and jet variability have their strongest impact on ozone gradients and variability.

4 Dynamical diagnostics methodology

In this section, we describe the dynamical diagnostics currently used in OCTAV-UTLS as well as the methodology for their generation. Figure 2 shows a timeline of the dynamical diagnostics available to date. Note that this timeline reflects the processing of the dynamical diagnostics and not the timeline of the measurement record, which in many cases extends to the current date.

Briefly, these dynamical diagnostics provide at each measurement time and location a comprehensive set of meteorological variables useful for characterizing the effects of dynamical variability on composition. The meteorological data used herein to compute the dynamical diagnostics are from the Modern-Era Retrospective Analysis for Research and Applications version 2 (MERRA-2) reanalysis (Gelaro et al., 2017). MERRA-2 is produced using version 5.12.4 of the Goddard Earth Observing System assimilation system using a 3D-FGAT (first guess at the appropriate time) with an incremental analysis update (Bloom et al., 1996) assimilation scheme to constrain the analyses (Lawless, 2010). The MERRA-2 dataset covers from 1980 to the present, providing fields every 3 h on a 0.625° by 0.5° longitude/latitude grid with 72 hybrid σ-pressure levels between the surface and 0.01 hPa. Its typical UTLS spacing is about 1.2 km. The approximate vertical resolutions for its entire vertical range can be found in Fig. 3 by Fujiwara et al. (2017). Between January 1980 and September 2004, MERRA-2 assimilates partial column O_3 retrievals from the Solar Backscatter Ultraviolet Radiometer instruments, and starting in October 2004, it assimilates O_3 profiles from Aura MLS and total column O_3 from the Ozone Monitoring Instrument (Wargan et al., 2017). MERRA-2 products have been extensively compared with those from other reanalyses and found to be well suited for UTLS studies (e.g., Manney et al., 2017, 2021a, b; Homeyer et al., 2022; Fujiwara et al., 2022; Tegtmeier et al., 2022).

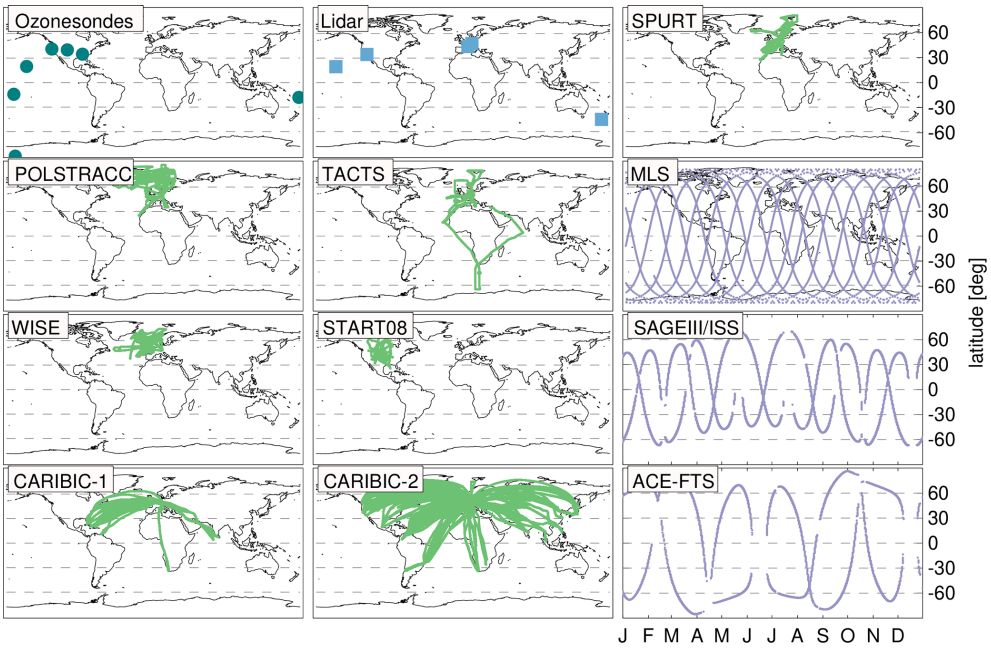

Figure 1. Locations of ozonesondes (teal circles) and lidars (blue rectangles), sampling of aircraft campaigns (light green), and representative sampling patterns for satellite instruments (MLS daily sampling pattern, SAGEIII/ISS and ACE-FTS yearly sampling patterns, all in purple).

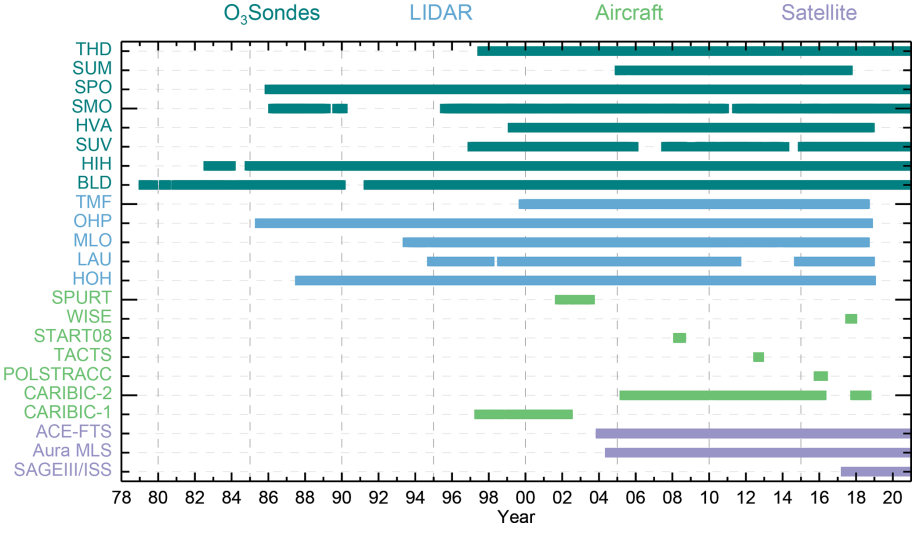

Figure 2. Dynamical diagnostics availability between 1979–2020 for the datasets considered within the OCTAV-UTLS SPARC activity.

When computing dynamical diagnostics as discussed in this section, it is important to use the same reanalysis fields for all the datasets to be used in a given study. This is to avoid introducing artifacts in the climatology and trend analyses from differences between the meteorological fields. For example, because of changes in assimilated datasets and different processing streams, discontinuities in the temperature and wind time series occur (Long et al., 2017). The magnitude and timing of these discontinuities vary between reanalyses and could confound the interpretation of studies using dynamical diagnostics derived from different reanalysis. Xian and Homeyer (2019) found when comparing WMO tropopauses derived from reanalysis fields with tropopauses derived from radiosonde data that in general, the MERRA-2 primary tropopause altitudes have a positive bias, while other reanalyses have negative biases. Millán et al. (2021) found, intercomparing dynamical tropopauses from multiple reanalysis fields, that root-mean-square daily altitude differences could be up to 1 km over most of the globe and greater than 2 km over Greenland, the Andes, Antarctica, and around

30° S and 30° N. Manney et al. (2017) showed comprehensive comparisons of five modern reanalyses for UT jets, the "subvortex" jet (see below), and multiple tropopauses, indicating generally good agreement in overall UT and subvortex jets characteristics, larger discrepancies in multiple tropopause characterization, and strong dependence of agreement in all diagnostics on the vertical grid resolution of the reanalyses. Manney and Hegglin (2018) evaluated long-term changes in UT jet latitude, altitude, and strength in the same reanalyses. While the signs of trends were usually the same, their magnitudes, uncertainty, and significance differed considerably, and some regions and seasons showed differences even in the signs of trends from different reanalyses in the Southern Hemisphere. Manney et al. (2021a) diagnosed relationships of UT jet variability to the El Niño–Southern Oscillation (ENSO) using three modern reanalyses including MERRA-2, finding overall good agreement in the relationships between UT jets and ENSO among them. Manney et al. (2021b) used MERRA-2 and two other reanalyses to characterize the Asian summer monsoon anticyclone (ASMA) and found an altitude-dependent positive bias in the MERRA-2 ASMA area with respect to the other reanalyses. A thorough reanalysis intercomparison can be found in the SPARC Reanalysis Intercomparison Project (S-RIP) Final Report (Fujiwara et al., 2022), of which Chaps. 7 and 8 (Homeyer et al., 2022; Tegtmeier et al., 2022) focus on the extratropical and tropical UTLS, respectively.

Thus, given these discontinuities, it is crucial to use the same reanalysis for all datasets throughout a given study. While using only one reanalysis cannot completely eliminate the impact of these discontinuities, it can ensure that their effects are consistent across all datasets studied. That is, the timing of these discontinuities is well documented, and it can be identified. If more than one reanalysis were used, the timing of discontinuities would be different, complicating the interpretation of such studies. That said, there is also value in repeating a study with meteorological fields from different reanalyses to study the sensitivity of the results to the uncertainties in the dynamical variables as recommended by S-RIP (Fujiwara et al., 2022).

The dynamical diagnostics are computed using the JEt and Tropopause Products for analysis and characterization (JETPAC) software. Originally, these algorithms were developed to process satellite measurements, but they have since been adapted to accommodate a diverse range of atmospheric measurements, including ozonesondes, lidars, and aircraft campaigns. Notably, this is the first time that all these records will be characterized consistently.

The JETPAC algorithms are described in detail by Manney et al. (2011, 2014, 2017, 2021a) and Manney and Hegglin (2018). For completeness, a review of the previously published use of JETPAC products for characterizing composition measurements is given here along with an update describing the current capabilities (for example, processing high-resolution datasets) and their applications. This review also describes the JETPAC algorithm as applied to characterizing measurement environments, as opposed to referring the reader to Manney et al. (2011), who describe a previous iteration of the algorithms for two satellite datasets, and Manney et al. (2014, 2017, 2021a) and Manney and Hegglin (2018), who use JETPAC products only on the reanalysis grids for dynamical studies. In other words, the previous publications do not give a full view of the current capabilities of JETPAC for characterizing composition measurements.

The dynamical diagnostics generated by JETPAC can be broken down into three categories: derived meteorological products, tropopause characterization, and UT jet and subvortex jet identification. JETPAC is modular, and other reanalyses besides MERRA-2 could be used in the future to verify that the results for measurement-location dynamical diagnostics are not reanalysis-dependent. When computing dynamical diagnostics for multiple datasets, it is also important to use the same code to compute such diagnostics. For example, other algorithms exist to derive equivalent latitude (e.g., Hoor et al., 2004; Hegglin et al., 2006; Añel et al., 2013), jet information (e.g., Strong and Davis, 2008; Spensberger and Spengler, 2020, and references therein), or tropopause information (e.g., Cohen et al., 2021; Homeyer et al., 2022, and references therein). All of these algorithms involve several assumptions, which are different in different algorithms, and also numerous interpolations, which may be done differently. Thus, significant differences could result simply from using a different code for different datasets.

4.1 Derived meteorological products

The derived meteorological products are reanalysis fields, such as potential temperature (θ), interpolated to the measurements' times and locations, as well as some derived meteorological products such as static stability (the gravitational resistance of the atmosphere to vertical displacements) and equivalent latitude (EqL). EqL is a quasi-Lagrangian coordinate defined as the geographical latitude encompassing the same area as the given potential vorticity (PV) contour (e.g., Butchart and Remsberg, 1986). EqL makes use of the conservation laws for potential vorticity for adiabatic frictionless flow. Under these conditions, PV is conserved and can be considered a passive tracer. In the stratosphere, this approximately holds for timescales of days to weeks. Here, tropospheric diabatic effects and turbulence do not play a significant role, and the timescales are short enough that radiation and large-scale downwelling do not dominate changes in PV. EqL is widely used in stratospheric studies (Brunner et al., 2006; Davis et al., 2017; Millán and Manney, 2017; Thomason et al., 2018; Manney et al., 2020, and references therein), as well as in UTLS studies to account for the local dynamical tropopause location (e.g., Strahan, 1999; Hoor et al., 2004; Engel et al., 2006; Hegglin et al., 2006; Bönisch et al., 2009; Krause et al., 2018). Table 4 lists the meteorological fields saved at each measurement location. The me-

teorological fields are interpolated linearly in time and bilinearly in latitude and longitude. Vertical interpolations are linear in log(θ) for PV or log(pressure) for other products. EqL is calculated on isentropic surfaces and interpolated linearly in log(θ). The isentropic surfaces used are a grid commensurate with the MERRA-2 vertical spacing, from which EqL is then interpolated to the final desired levels (typically the potential temperatures of the measurement locations for the products described herein).

An important product from the reanalyses is the assimilated ozone at the measurement times and locations. This product not only facilitates studies of the reanalyses' representation of ozone but also facilitates sampling biases studies by allowing comparison of the complete reanalysis fields mapped into a given coordinate system versus the assimilated ozone at the measurement locations in such coordinate system. For example, Chap. 7 of the S-RIP report (Homeyer et al., 2022) illustrates that sampling biases can be a confounding factor, even with dense sampling such as from MLS. Conducting sampling bias studies can aid in evaluating the comparability of datasets with very dissimilar sampling patterns, including those presented herein (see Fig. 1). Moreover, sampling differences can result in significant biases in the inferred magnitude of ozone trends, as highlighted by Millán et al. (2016).

As an example, Fig. 3 shows the ozonesonde measurements (ozone, temperature, and wind speed) and MERRA-2-derived meteorological products (ozone, temperature, wind speed, and static stability) for the launches on 21 December 2009 and 12 January 2010 from Boulder, Colorado. On 21 December, MERRA-2 fields overestimate the ozone and wind speed, while on 12 January, the derived meteorological products display excellent agreement with the ozonesonde measurements.

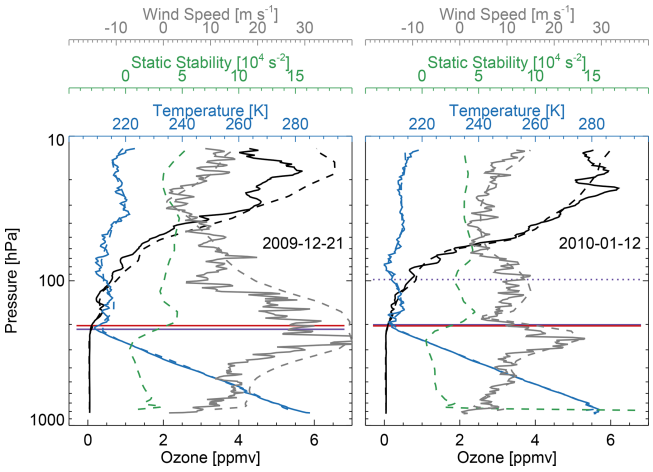

Figure 3. Ozonesonde measurements (solid) and MERRA-2 derived meteorological products (dashed) for the launches in 21 December 2009 and 12 January 2010 from Boulder, Colorado. Red lines show the 4.5 PVU dynamical tropopause and purple lines the WMO (thermal) tropopause (dotted purple lines show the secondary thermal tropopause).

4.2 Tropopause characterization

An accurate depiction of the tropopause is important because it acts as a dynamical barrier separating strongly stratified stratospheric air from well-mixed tropospheric air, thus resulting in strong gradients in trace gases across the tropopause (e.g., Pan et al., 2004; Hoor et al., 2004; Hegglin et al., 2009). At each measurement time and location, JETPAC identifies the thermal tropopause using the WMO definition (e.g., Homeyer et al., 2010), that is, where the temperature lapse rate falls below 2 K km^{-1} for at least 2 km. We also use JETPAC to identify the dynamical tropopauses using four PV values (2, 3.5, 4.5, and 6 potential vorticity units). PV has been widely used to identify the tropopause location since stratospheric air possesses higher values of PV than tropospheric air, and changes in static stability result in strong vertical PV gradients at the tropopause (e.g., Morgan and Nielsen-Gammon, 1998). Since PV does not provide a well-defined tropopause near the tropics (e.g., Holton et al., 1995), these dynamical tropopauses are commonly defined by an isentropic surface (typically 380 K) wherever the PV contour definition would place it at a higher potential temperature (e.g., Schoeberl, 2004; Manney et al., 2011). The four PV values used for these dynamical diagnostics span the range of most commonly used values in the literature (e.g., Hoskins et al., 1985; Highwood et al., 2000; Schoeberl, 2004; Randel et al., 2007; Kunz et al., 2011a; Pan et al., 2012) and are consistent with PV gradients in the extratropics that arguably best reflect the dynamical barrier and tracer gradients (Kunz et al., 2011a, b). For the calculations herein, JETPAC searches for tropopauses above 1.5 km and for pressure levels smaller than 600 hPa, to avoid identifying boundary layer inversions as tropopauses.

In addition to the primary tropopause, multiple tropopauses are also identified by JETPAC above the primary tropopause every time their particular definition is fulfilled. Note that to identify multiple thermal tropopauses, we only require the temperature lapse rate to drop below 2 K km^{-1} as opposed to 3 K km^{-1} as defined by the WMO (WMO, 1957). Randel et al. (2007) showed that the frequency of double thermal tropopause occurrence is dependent on the chosen lapse rate threshold, with 2 K km^{-1} resulting in better agreement when comparing double tropopauses derived from (relatively coarse-resolution) reanalyses with those derived from high-resolution datasets using the strict WMO definition. Multiple dynamical tropopauses are also reported and physically represent regions of tropopause folding, which are often associated with stratosphere-troposphere exchange.

In addition to the derived meteorological products, Fig. 3 also displays the location of the 4.5 PVU and WMO tropopauses. On 21 December 2009, there was only one

Table 4. Dynamical diagnostic products.

Derived meteorological products[a]	
Pressure	Temperature
Zonal wind	Meridional wind
Potential temperature	Geopotential height
Altitude	Potential vorticity
Scaled PV	Relative vorticity
Lapse rate	Static stability
Equivalent latitude[d]	Normalized horizontal (isentropic) PV gradient[d]
Horizontal (isobaric) temperature gradient	Montgomery stream function[e]
Montgomery stream function	Assimilated ozone
Tropopause characterization[b]	
Number of tropopauses	Altitude
Pressure	Potential vorticity
Potential temperature	Static stability
Lapse rate	
Jet identification[c]	
Jet location (lat–long)	Jet types
Pressure	Temperature
Zonal wind	Meridional wind
Potential vorticity	Relative vorticity
Lapse rate	Static stability
Potential temperature	

[a] Variables saved at each measurement location. [b] Information saved at each tropopause (either thermal or dynamical as well as primary, secondary, and tertiary, etc.) location. [c] Information saved at the jets' maximum and edges (poleward, equatorward, inner, outer). [d] Calculated on isentropic surfaces. [e] Computed using the approximation MSF $= gz + c_pT$, where g is Earth's gravity, z is the height of the isentropic surface, c_p is the specific heat of air at constant pressure, and T is the atmospheric temperature.

tropopause associated with the profile (at 204 and 216 hPa for the 4.5 PVU and WMO tropopause, respectively), while on 12 January 2010, two WMO tropopauses were identified by JETPAC (at 201 and 98 hPa), coincident with strong gradients of static stability. On 12 January 2010, the locations of the primary WMO and 4.5 PVU tropopauses are almost the same. This figure also shows tropopause inversions (e.g., Birner et al., 2002, 2006). The tropopause inversion layer (TIL) is a shallow layer just above the tropopause, corresponding to a local maximum in static stability. These inversions often occur in the same regions and seasons as multiple tropopauses (e.g., Grise et al., 2010; Peevey et al., 2014; Schwartz et al., 2015). The representation of the TIL showcases the ability of modern reanalyses to capture the sharp gradients associated with such inversions (e.g., Gettelman and Wang, 2015; Kedzierski et al., 2016; Wargan and Coy, 2016). The ability to properly represent these inversion layers is important to define coordinates capable of capturing the trace gas gradients in the UTLS.

For many of the composition datasets, the latitude, longitude, and measurement time change with pressure/altitude; for example, during an ozonesonde measurement, the balloon drifts from the launch location, or for a limb measurement the latitude–longitude position of the tangent height may change significantly as the satellite orbits the Earth while the instrument scans the atmosphere. As such, in principle, we could provide tropopause information at every single measurement point along the balloon ascent/satellite measurements; however, this may generate a large amount of mostly redundant information and can result in very large files, so we instead provide just one tropopause characterization.

Figure 4 shows examples of how we determine a unique tropopause for a balloon ascent as well as for satellite scans whose locations vary significantly with altitude.

- First, we compute the tropopause information (based on the interpolated reanalysis fields) for the measurements below 30 km as their lat–long change with height along the balloon ascent or along the limb scan (gray dots in Fig. 4).
- Then, we compute the mean of the primary tropopauses computed (indicated by purple arrows in Fig. 4).
- This mean tropopause value typically does not coincide exactly with a measurement altitude (best seen in the ACE-FTS panel in Fig. 4 because of the coarser retrieval grid of its measurements).

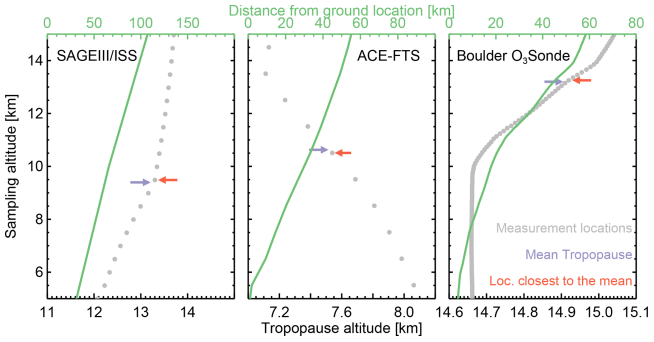

Figure 4. SAGEIII/ISS, ACE-FTS, and ozonesonde examples of the primary WMO tropopause variation through the balloon ascent/satellite measurements. The WMO tropopause characterization used is the one from the measurement location closest to the average tropopause through the balloon ascent/satellite measurements. An analogous procedure is used to identify unique dynamical tropopauses through the balloon ascent/satellite measurements. For satellites, distance from the ground location refers to the distance from the lowest available retrieval level.

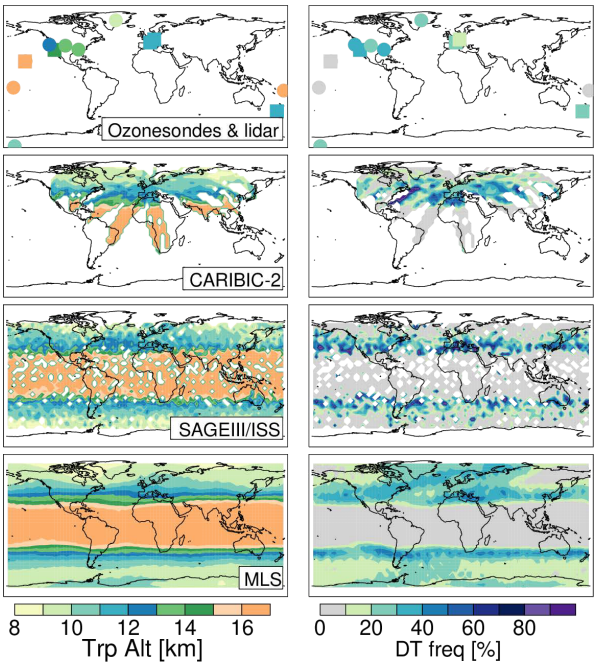

Figure 5. Left: climatological MERRA-2 WMO primary tropopause altitude sampled at ozonesondes (circles), lidar (rectangles), CARIBIC-2, SAGEIII/ISS, and MLS measurements. Right: climatologies of MERRA-2 WMO double tropopause occurrence frequencies for the same datasets. MLS and SAGEIII/ISS display 2018 data, and CARIBIC-2, ozonesonde, and lidar show data post 2005.

– We thus find the measurement location where the tropopause value is closest to the mean value just computed (indicated by red arrows in Fig. 4). The tropopause characterization for that level (and hence geographic location) is selected as the most representative tropopause characterization of the entire balloon ascent or the entire limb scan.

– We repeat this procedure for each tropopause definition.

To explore the tropopause characterization further, Fig. 5 shows maps of the mean WMO tropopause altitude for several datasets, as well as the double WMO tropopause occurrence frequency. The representation of the altitude of the WMO primary tropopause and the WMO double tropopause frequency depends on the time and sampling patterns of the measurements. The most noticeable examples are the high values of double tropopause occurrence (above 80 %) in the CARIBIC-2 dataset in the North Atlantic Ocean close to the US coast and the 20 %–30 % double tropopause occurrence around Greenland only present for the MLS measurements despite CARIBIC-2 and SAGEIII/ISS measuring at least part of that region. The list of tropopause characteristics saved at each measurement location can also be found in Table 4.

4.3 UT jet and subvortex jet identification

At each measurement longitude, upper tropospheric jet cores are identified in latitude/vertical coordinate slices where the reanalysis wind speed maximum exceeds 40 m s^{-1}. The jet boundaries are the grid points surrounding that core (both vertically and horizontally) where the wind speed drops below 30 m s^{-1}. When there is more than one wind speed maximum greater than 40 m s^{-1} within a given 30 m s^{-1} contour, they are identified as separate cores if the minimum wind speed between them is at least 30 m s^{-1} less than the wind speed value at the strongest core or if the latitude distance between them is greater than 15°. These criteria were chosen to approximate the selections that would be made by visual inspection. As an example, following Manney et al. (2011), Fig. 6 illustrates the jet identification. This figure shows two cross-sections of wind speed, one in Southern Hemisphere spring and one in the Northern Hemisphere winter. In both cross sections there are two 40 m s^{-1} maxima within a given 30 m s^{-1} contour. In the Southern Hemisphere, they are cataloged as one jet core (identified as the subtropical jet (STJ)), while in the Northern Hemisphere they are cataloged as two jet cores (N1 and polar jet (PJ)).

In each hemisphere, JETPAC identifies the subtropical jet as the jet core closer to the Equator for which the WMO tropopause altitude at the equatorial edge is greater than 13 km and for which the tropopause altitude is at least 2 km lower on its opposite (poleward) side. The polar jet is defined as the strongest jet core poleward of the subtropical jet or poleward of 40° latitude if no subtropical jet is identified. These criteria ensure that, in general, the identified subtropical jets are the ones close to the tropopause break (i.e., the abrupt drop in the height of the WMO tropopause while transitioning from the tropics to midlatitudes), consistent with primarily radiative driving, while the polar jets are consis-

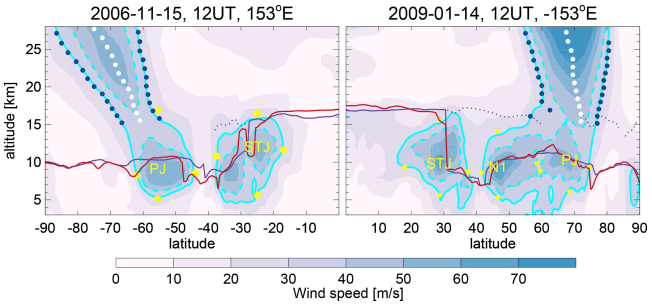

Figure 6. Cross-sections of MERRA-2 wind speed with jet and tropopause classification information overlaid. Yellow letters/numbers indicate the locations of jet cores; lowest numbers are for strongest jets in each hemisphere; yellow dots indicate the identified locations of the edges of the jet region (at grid points, thus not exactly matching contours). The red line shows the 4.5 PVU dynamical tropopause and the purple line the WMO (thermal) tropopause (dotted purple lines show the secondary thermal tropopause). White dots show the subvortex jet maximum and blue dots the edges of the subvortex jet. Figure based on Manney et al. (2011).

tent with primarily eddy driving. Any other jet cores (up to five at the longitude/time of a given measurement) are also cataloged; the catalog is ordered by decreasing jet core wind speed, with subtropical and polar jets indicated by a flag in the dynamical diagnostic files.

In each hemisphere, JETPAC identifies the subvortex jet core as the most poleward westerly reanalysis wind speed maximum, as long as it exceeds 30 m s^{-1}, at each model level above near 300 hPa (the white dots in Fig. 6). The subvortex edges are the location of the 30 m s^{-1} wind speeds on both sides of the subvortex core (i.e., poleward and equatorward, the blue dots in Fig. 6). Between 300 and 80 hPa, the bottom of the subvortex jet is distinguished from the top of an upper tropospheric jet as the lowest altitude at which the wind speed of the jet is still decreasing with decreasing altitude. Once the upper tropospheric jets and subvortex jet are identified, we catalog the distances (vertically in pressure, height, and potential temperature and horizontally in latitude) from them to the measurement locations. Table 4 lists all the jet and subvortex parameters saved from JETPAC.

As we did for the tropopause identification, we provide just one jet and subvortex identification per balloon ascent/limb scan. This identification is similar to the unique tropopause identification explained before, and it is computed as follows: first, we compute the UT jet and subvortex jet information for all measurements through a balloon ascent or limb scan. Then, we compute the mean jet core wind speed of the strongest UT jet throughout the locations along a balloon ascent or limb scan. The mean jet core wind speed typically does not coincide exactly with the jet core wind speed at any of the measured locations, so we identified the measured location with jet core wind speed closest to that mean jet core wind speed. The information at this measured location is taken to be the best representation of the UT jet and subvortex jet information for the entire balloon ascent or limb scan.

5 Coordinate systems

The dynamical diagnostics discussed here are the first comprehensive and consistent set of diagnostics across multiplatform datasets. In addition to allowing mapping of the datasets into additional conventional coordinate systems (for example, the MLS pressure-based dataset into altitude or the SAGEIII/ISS altitude-based dataset into pressure), these diagnostics allow mapping of such datasets into several dynamically based latitude-like horizontal coordinates and altitude-like vertical coordinates (Manney et al., 2011). Potentially useful horizontal coordinates include latitude, equivalent latitude, and latitude distance from the subtropical or polar jet. Vertical coordinates include altitude, pressure, potential temperature, altitude, or potential temperature from a jet core and altitude or potential temperature from a tropopause. Table 5 shows specific horizontal and vertical coordinate combinations enabled by the dynamical diagnostics.

Mapping into a given coordinate system can be performed by simply averaging the composition measurements within coordinate bins. Variability within a given bin can be characterized by standard deviations, median, minimum/maximum values, and percentiles, etc. The number of points in each bin can be easily stored to ensure an adequate number of data points within the bins and to facilitate combining mapped fields into longer averaging periods. Figure 7 displays various ozone datasets mapped using latitude versus altitude, a commonly utilized coordinate system. These datasets were selected to showcase the variety of records included on OCTAV-UTLS: MLS and SAGEIII/ISS showcase satellite measurements with dense and sparse sampling, and CARIBIC-2 illustrates aircraft measurements, while the Boulder and Table Mountain measurements represent the ozonesonde and lidar records, respectively. As expected, ozone is low and well mixed in the troposphere, increasing in the lower stratosphere due to photochemical production.

The sampling of each record is evident in the zonal means presented here. MLS, with its dense sampling and near-global coverage (82° S–82° N), provides a comprehensive perspective of global ozone fields, capturing the climatological view of the subtropical jet and subvortex jet (black contours; see Fig. 6 for reference). However, MLS suffers from a lack of coverage below ∼ 10 km and coarser vertical resolution compared to the other datasets used here. On the other hand, SAGEIII/ISS offers sampling in the upper troposphere with measurements down to 5 km, with better vertical resolution, but is limited to measurements between 60° S and 60° N. The distorted wind contours in comparison to MLS illustrate the greater impact of sampling biases than for MLS.

Table 5. Coordinate systems enabled by the dynamical diagnostics.

	Altitude (z)	Pressure (p)	Potential temperature (θ)	z relative to tropopause	θ relative to tropopause	z relative to STJ	θ relative to STJ	z relative to PJ	θ relative to PJ
Latitude	•	•	•	•	•	•	•	•	•
Equivalent latitude	•	•	•	•	•	•	•	•	•
Latitude from STJ	•	•	•	•	•	•	•		
Latitude from PJ	•	•	•	•	•			•	•

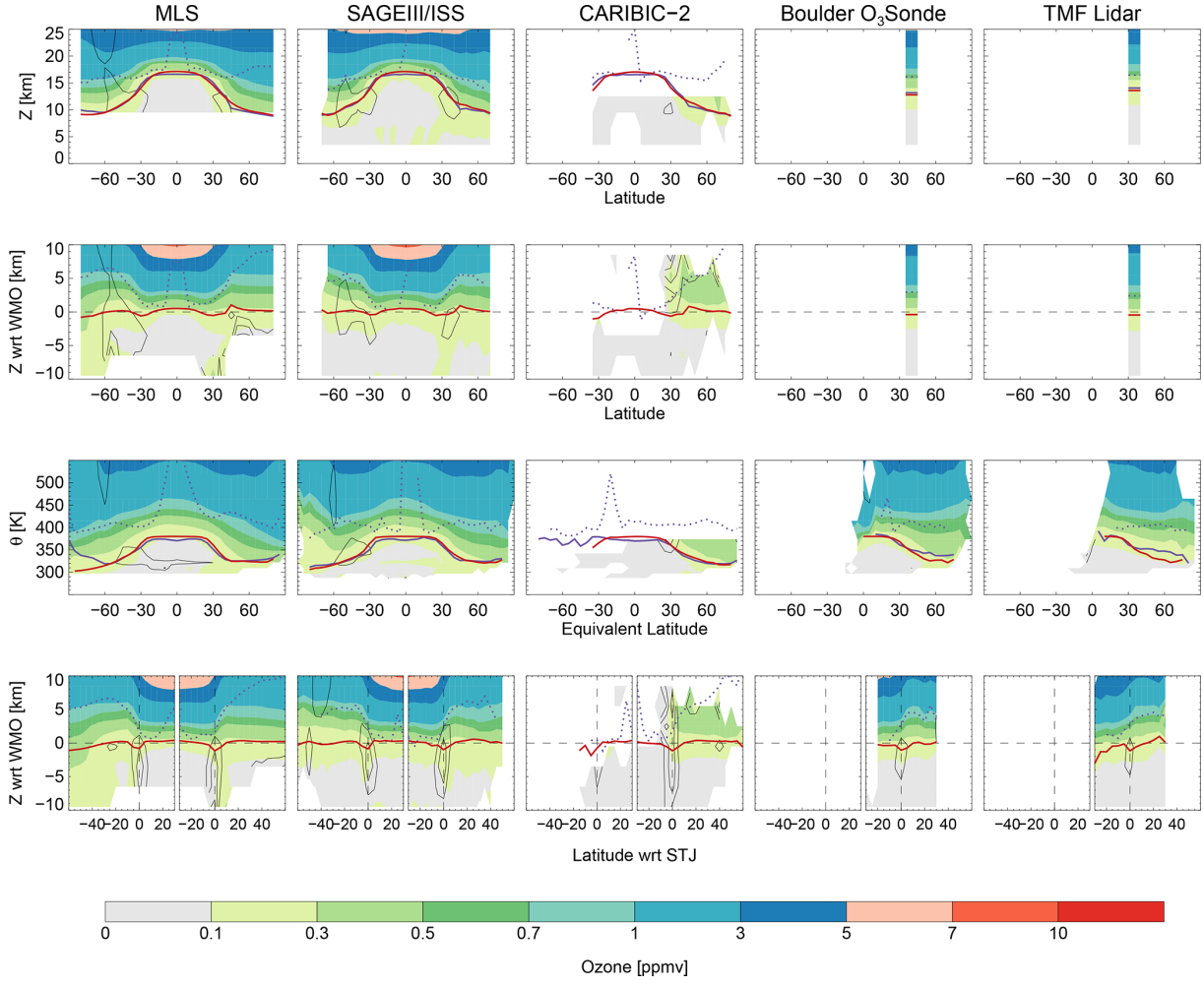

Figure 7. Climatological MLS, SAGEIII/ISS, CARIBIC-2, Boulder ozonesonde, and Table Mountain tropospheric ozone lidar data in different coordinate systems. MLS and SAGEIII/ISS display 2018 data, and CARIBIC-2, Boulder ozonesonde, and Table Mountain lidar show data post 2005. Red lines show the 4.5 PVU dynamical tropopause, and purple lines the WMO (thermal) tropopause (dotted purple lines show the secondary thermal tropopause). The black contours show wind speed values of 30, 40, and 50 m s^{-1}. Note that differences in their representation in comparison with MLS suggest sampling biases. Datasets were binned on a 5° horizontal grid and a 5 km or 5 K grid. Note that in the top two rows, the ozonesondes and lidar measurements (that only sample one latitude bin) have been replicated in the adjacent latitude bins to improve visibility.

CARIBIC-2 measurements are restricted to flight levels, mostly situated at altitudes below 12 km, near the extratropical tropopause. These measurements, due to their high-frequency observation rate, capture much finer details that are not resolved by satellite products. As such, it provides an exceptional perspective for studying tropopause-related processes in this region, but its coverage is limited elsewhere. Finally, ozone measurements obtained by ozonesondes and lidars provide superior vertical resolution but are confined to their specific measurement locations. To enhance their visi-

bility, we have replicated the ozonesonde and lidar measurements in the adjacent latitude bins in Fig. 7 (top).

The different sampling of each of these datasets may contribute to biases/artifacts and confound the interpretation of the results. To better understand this issue, OCTAV-UTLS aims to characterize the sampling biases of these datasets by comparing ozone reanalysis fields that are interpolated to the measurement times and locations (included in the dynamical diagnostics discussed herein) with the raw reanalysis fields (similar to the approach used in previous studies, e.g., Toohey et al., 2013; Millán et al., 2016).

Figure 7 also shows the datasets mapped into latitude versus altitude with respect to the WMO tropopause. Tropopause coordinates allow for the separation of tropospheric and stratospheric air and remove variability caused by differences in tropopause height, allowing better characterization not only of troposphere to stratosphere gradients but also of errors associated with each regime. It has been shown that using tropopause coordinates greatly reduces the scatter around the tropopause, revealing a sharp gradient between tropospheric and stratospheric air masses (e.g., Pan et al., 2004; Hoor et al., 2004; Hegglin et al., 2006, 2009). This coordinate system has been used to validate ozone measurements from several satellite instruments against coincident measurements (e.g., Monahan et al., 2007; Pittman et al., 2009). Furthermore, Hegglin et al. (2008) argue that this coordinate system can be used in a climatological manner, enabling the inclusion of all available measurements as opposed to just spatiotemporally coincident ones, thus improving validation statistics especially for instruments with less dense sampling patterns.

The impact on coverage of the tropopause mapping can be seen in particular in MLS and in CARIBIC-2. Although MLS shows very few measurements below the tropopause in the extratropics in the latitude/altitude view, mapping with respect to the tropopause allows separation of individual measurements that were taken above and below the tropopause. This shows that MLS does on occasion sample below the extratropical tropopause. Similarly, in the extratropics, CARIBIC-2 covers only a few kilometers above the tropopause in the latitude/altitude mapping, but the use of tropopause coordinates shows that it covers air masses that are high above the local tropopause (e.g., above deep folds) and thus samples deep stratospheric air.

Figure 7 also shows the datasets mapped into equivalent latitude versus potential temperature coordinates. The benefits of using EqL / θ coordinates (or PV / θ) for data comparisons are well established (e.g., Hegglin et al., 2006; Lait et al., 2004; Velazco et al., 2011). Trace gases with transport timescales significantly shorter than their chemical timescales are well mixed along EqL (or PV) contours on isentropic surfaces (e.g., Leovy et al., 1985), which facilitates comparisons of non-coincident measurements taken in the same air mass, in addition to providing criteria to filter out coincident measurements that were taken in different air masses (a common occurrence in regions of strong PV gradients such as the stratospheric vortex edge or the tropopause) (e.g., Michelsen et al., 2002; Lumpe et al., 2002; Chiou et al., 2004; Lumpe et al., 2006; Velazco et al., 2011; Griffin et al., 2017; Ryan et al., 2017; Bognar et al., 2019).

All instruments show expanded "condition space" coverage when mapped in EqL / θ coordinates (e.g., Schoeberl et al., 1995; Manney et al., 2009, and references therein); this is particularly noticeable for the ozonesonde and lidar datasets, which, while physically measuring at a single location, show a broad distribution of ozone values typical of a wide range of dynamical conditions found throughout the respective hemisphere they are located in. Figure 8a and c depict a normalized count of the ozonesonde and lidar coverage in equivalent latitude. The vertical dashed lines display the geographical latitude for the ozonesonde launches or the lidar locations (noting that geographical and equivalent latitude have completely different meanings and implications). Any deviations observed between these lines and the maximum normalized count (i.e., 1) indicate that the respective datasets are situated in a region of significant dynamical variability, which leads to diabatic PV modification and thus a shift in equivalent latitude, such as the South Pole and Summit (Greenland) ozonesondes or the Table Mountain lidar measurements. As shown, the expanded space can cover from 11 to 30° (determined as the half-width of the normalized counts). Note that, in Fig. 7, all other records show coverage improvements, with SAGEIII/ISS covering most of the globe, CARIBIC-2 extending its coverage throughout the Northern Hemisphere, and MLS covering the entire globe.

However, studies have shown that PV or EqL coordinates must be used with caution in the upper troposphere because adiabatic PV conservation is violated particularly by phase transitions of water as well as regional turbulence (in particular in the vicinity of the jet cores) and a lack of a single simply connected approximately circumpolar transport barrier (e.g., Manney et al., 2011; Pan et al., 2012; Jin et al., 2013; Kaluza et al., 2021). In this region, other coordinate systems may map ozone differently and thus provide additional insights for interpreting the data. Figure 7 shows the datasets mapped into latitude with respect to the STJ versus altitude with respect to the WMO tropopause. This coordinate combination almost completely segregates the ozone measurements taken in different air masses by separating tropospheric and stratospheric air in the vertical and air on either side of the transport barrier represented by the subtropical jet in the horizontal. This separation is most evident in the CARIBIC-2 panel. As discussed by Manney et al. (2011), the horizontal jet coordinate reorders the data geometrically and thus highlights ozone, tropopause height, and strong local horizontal PV gradients across the jets in the latitude region strongly influenced by those jets; EqL (or PV) provides a complementary view that may not highlight the strongest PV gradients because of regional variations in the strength and position (in EqL) of the jet but helps identify various physi-

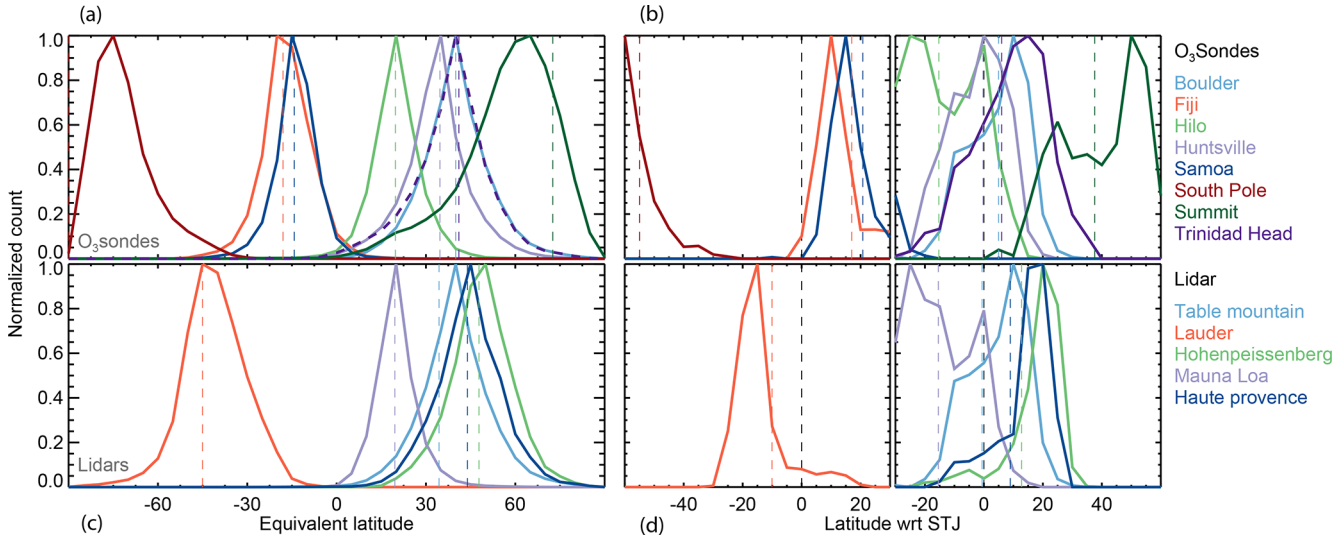

Figure 8. (a, c) Equivalent latitude range covered by the ozonesondes **(a)** and lidars **(c)**. Vertical dashed lines display the actual latitude position for each dataset as listed in Table 1. **(b, d)** Range covered by the same datasets but in latitude with respect to the subtropical jet. Vertical dashed colored lines display the dataset latitude with respect to a STJ climatological position of −35° S and 35° N. A vertical black line indicates the position of the subtropical jet (i.e., 0) in this coordinate system. Note that these normalized counts include information from multiple heights, so the coverage for specific heights could differ slightly.

cal processes influencing the trace gas distributions, such as mixing related to diabatic motions, and does, as mentioned above, also help in distinguishing tropospheric and stratospheric air.

Note that when referring to latitude with respect to the STJ, all instruments show an expanded measurement space, which is again most noticeable for the ozonesonde and lidar datasets. MLS, with its denser sampling, has full sampling of the region near the subtropical jets, as indicated by the concentric wind contours (black line) around the zero line. Figure 8b and d also show the extent of this coverage for the ozonesondes and lidars.

In addition to the composition measurements, we can map derived meteorological products such as winds, temperature, ozone, PV, potential temperature, and static stability into the same dynamically based coordinates. Figure 9 is an example of this type of mapping, showing MERRA-2 temperature fields interpolated to the measurement times and locations for several datasets mapped in the same coordinates shown in Fig. 7. Sampling biases are more obvious for temperature. Differences up to 7 K can be seen in comparing the ozonesonde and lidar datasets (when using EqL and latitude with respect to STJ coordinates) with MLS data. MLS has relatively dense sampling (see Fig. 1), which should minimize its sampling biases (Toohey et al., 2013; Millán et al., 2016) at least in the stratosphere; nevertheless, Homeyer et al. (2022) showed that even relatively dense MLS sampling resulted in significant biases in assimilated ozone fields with respect to the reanalysis fields on their native high-resolution latitude–longitude grids. As was the case for ozone, to fully understand these differences, the sampling biases need to be characterized. Figures A1, A2, A3, and A4 show examples of other datasets.

6 Summary and future directions

Understanding long-term changes in UTLS ozone is exceptionally challenging, in part because of the impact of the spatial and temporal variability of the jet streams and tropopause locations that are instrumental in controlling trace gas distributions. As part of the SPARC OCTAV-UTLS activity, we have generated dynamical diagnostics for multi-platform (ozonesondes, lidars, aircraft campaigns, and satellite) ozone records that allow such datasets to be mapped consistently into dynamical coordinates.

These dynamical diagnostics are computed with the well-established JETPAC software (Manney et al., 2011, 2014, 2017; Manney and Hegglin, 2018). They can be broken down into three categories:

- *Derived meteorological products*. Meteorological fields are interpolated to the measurement times and locations.
- *Tropopause characterization*. Tropopause information (either thermal or dynamical, as well as primary, secondary, and tertiary, etc.) is given at the measurement times and locations.
- *UT jet and subvortex jet identification*. UT jet and subvortex jet cores are identified and cataloged in latitude/height slices at each measurement longitude.

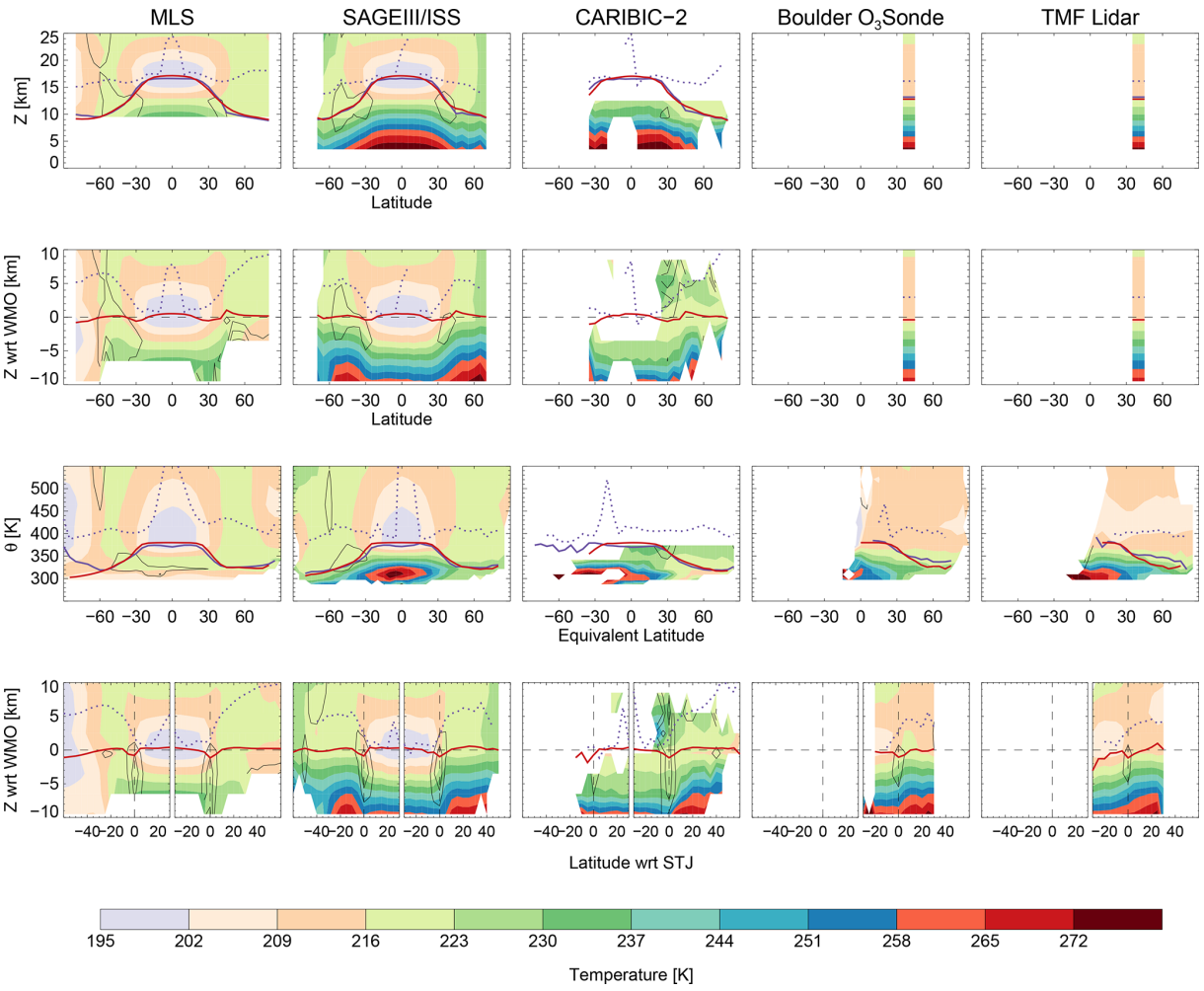

Figure 9. MERRA-2 temperature sampled at MLS, SAGEIII/ISS, CARIBIC-2, Boulder ozonesonde, and Table Mountain lidar measurements in different coordinate systems. MLS and SAGEIII/ISS panels display 2018 data, and CARIBIC-2, Boulder ozonesonde, and Table Mountain lidar panels show data post 2005. Red lines show the 4.5 PVU dynamical tropopause and purple lines the WMO (thermal) tropopause (dotted purple lines show the secondary thermal tropopause). The black contours show wind speed values of 30, 40, and 50 m s^{-1}. Note that differences in their representation in comparison with MLS suggest sampling biases. Datasets were binned on a 5° horizontal grid and a 5 km or 5 K grid.

Mapping multi-platform datasets into different coordinate systems will help us understand processes controlling UTLS ozone regionally and globally, as well as at seasonal timescales and longer. Suitable dynamical coordinates, such as tropopause coordinates and jet-based coordinates, will help us separate air masses with distinct characteristics, such as the tropospheric air where ozone is low and well mixed and stratospheric air where it increases with height. Further, using dynamical coordinates allows for separation of variability arising from different mechanisms, such as dynamical versus chemical processes.

Future OCTAV-UTLS studies on ozone will do the following:

- Investigate which dynamical coordinates better homogenize the mapped measurements, that is, which ones best segregate air in regions separated by geophysical transport barriers (for example, the tropopause) and thus provide the most comparable results within a given bin for non-coincident measurements. A paper on this topic is already on preparation. An illustrative example is shown on Fig. 10a for the WISE campaign using the relative standard deviation (RSTD; i.e., the standard deviation divided by the mean) as a metric to assess the variability in different coordinate systems. As expected, the dynamical coordinates display a smaller RSTD.

- Explore how sampling biases can confound the intercomparability of these records. These biases will be explored by comparing the ozone reanalysis fields interpolated to the measurement times and locations of the dynamical diagnostics discussed here to the raw reanal-

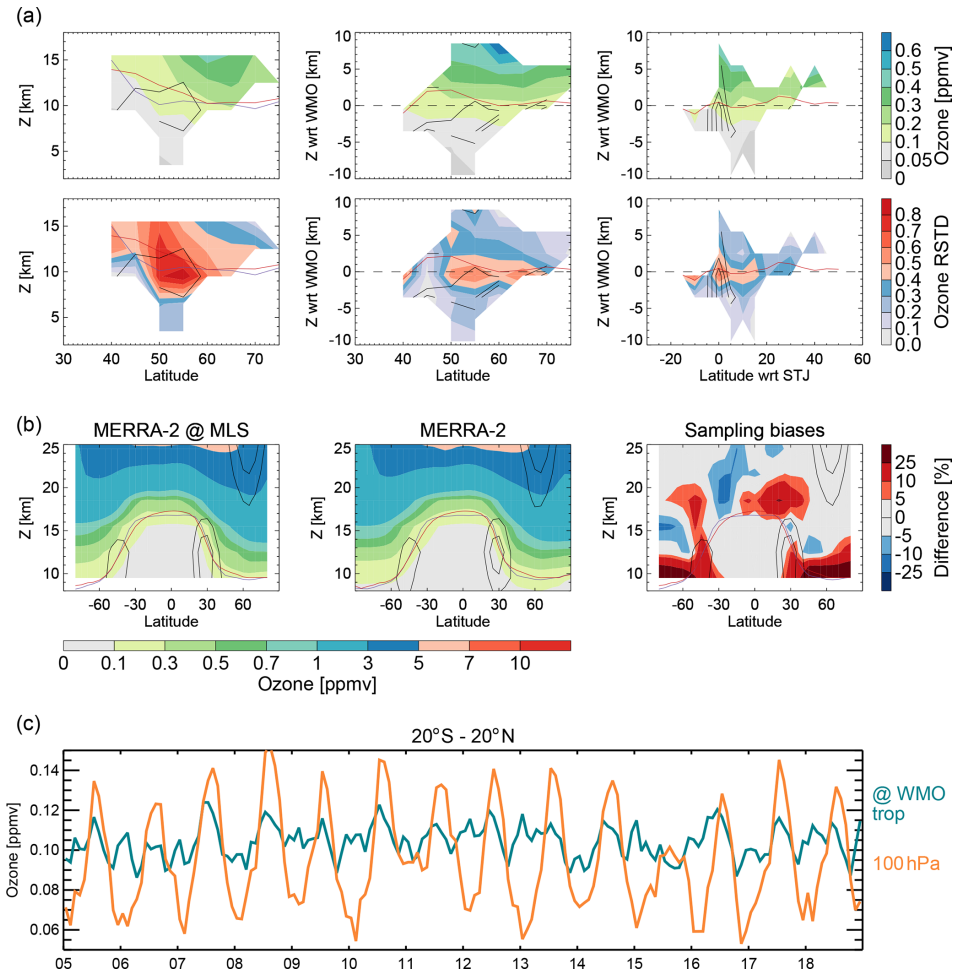

Figure 10. Illustrative examples of future OCTAV-UTLS studies. **(a)** WISE ozone data mapped into different coordinate systems (top) and their corresponding relative standard deviation (bottom). **(b)** January 2005 sampling biases as a function of latitude and altitude as computed using MERRA-2 fields interpolated at the MLS locations (i.e., one of the fields included in the dynamical diagnostics discussed here) versus the raw MERRA-2 fields. In **(a)** and **(b)**, red lines show the 4.5 PVU dynamical tropopause and purple lines the WMO (thermal) tropopause. Black contours show wind speed values of 30, 40, and 50 m s^{-1}. **(c)** MLS time series at 20° S–20° N at 100 hPa and at 0 km with respect to the WMO tropopause.

ysis fields. Additionally, this study will explore which coordinates can, if any, reduce sampling biases. As an example, Fig. 10b shows the MLS sampling biases for January 2005.

– Analyze the impact of dynamical coordinates on quantification of long-term trends. The aim is to identify regions where dynamical coordinates can reduce the uncertainty associated with such trends. As an example, Fig. 10c shows MLS 20° S–20° N time series at 100 hPa as well as at the WMO tropopause. As shown, the time series at 100 hPa displays much larger amplitude variations that are related to the annual cycle of the 100 hPa pressure surface with respect to the tropopause, which results in sampling different fractions of stratospheric and tropospheric air in different seasons. Interannual differences in these variations are also likely related to changes in the relative altitudes of the 100 hPa isobaric surface and the tropopause.

Uncertainties arising from differences between reanalysis fields from different centers will also be examined by comparing the results when using different reanalyses as recommended by the SPARC Reanalysis Intercomparison Project. Other datasets, such as more ozonesondes, IAGOS-CORE, the Gimballed Limb Observer for Radiance Imaging of the Atmosphere (GLORIA), the Michelson Interferometer for Passive Atmospheric Sounding (MIPAS), the Optical Spectrograph and InfraRed Imager System (OSIRIS), and the Ozone Mapping Profile Suite (OMPS), may also be processed with JETPAC for use in studies that combine the most comprehensive set of measurements and thus maximize spatiotemporal coverage. Some of these additional datasets may

be particularly useful when analyzing trace gases that are not measured by as many different platforms as ozone.

Ultimately, these dynamical diagnostics will allow satellite, aircraft, balloon, and ground-based observations of different long-lived and also shorter-lived trace gases to be studied in a physically consistent way in order to understand the impact of the physical processes (whether chemical or dynamical) driving trace gas variability on the observed UTLS trends as viewed by the different sensors on different platforms. The dynamical diagnostics and mapping techniques discussed herein can be used with all other trace gases measured by any platform; water vapor and carbon monoxide are among the species that will be a future focus of OCTAV-UTLS studies. For example, within OCTAV-UTLS, Jeffery et al. (2022) constructed water vapor and ozone climatologies using equivalent latitude and potential temperature tropopause-relative coordinates in an effort to best represent the distribution of these gases in the UTLS.

Appendix A: Other Datasets

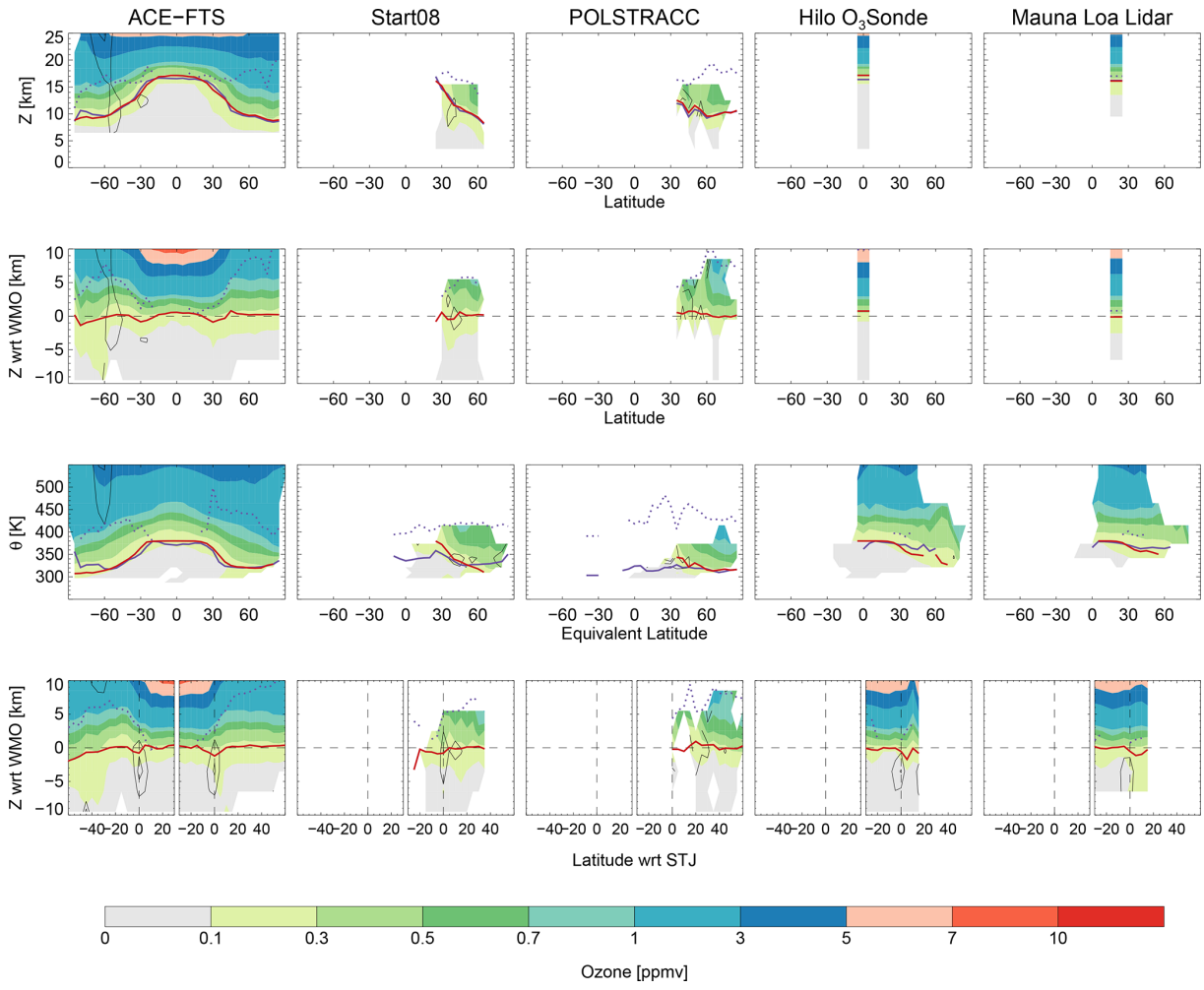

Figure A1. Climatological ACE-FTS, START08, POLSTRACC, Hilo ozonesonde, and Mauna Loa ozone data in different coordinate systems. ACE-FTS panel displays 2018 data, Hilo ozonesonde and Mauna Loa lidar show data post 2005, and START08 and POLSTRACC display all their available data. Red lines show the 4.5 PVU dynamical tropopause and purple lines the WMO (thermal) tropopause (dotted purple lines show the secondary thermal tropopause). The black contours show wind speed values of 30, 40, and 50 $\mathrm{m\,s^{-1}}$. Note that differences in their representation in comparison with MLS suggest sampling biases. Datasets were binned on a 5° horizontal grid and a 5 km or 5 K grid.

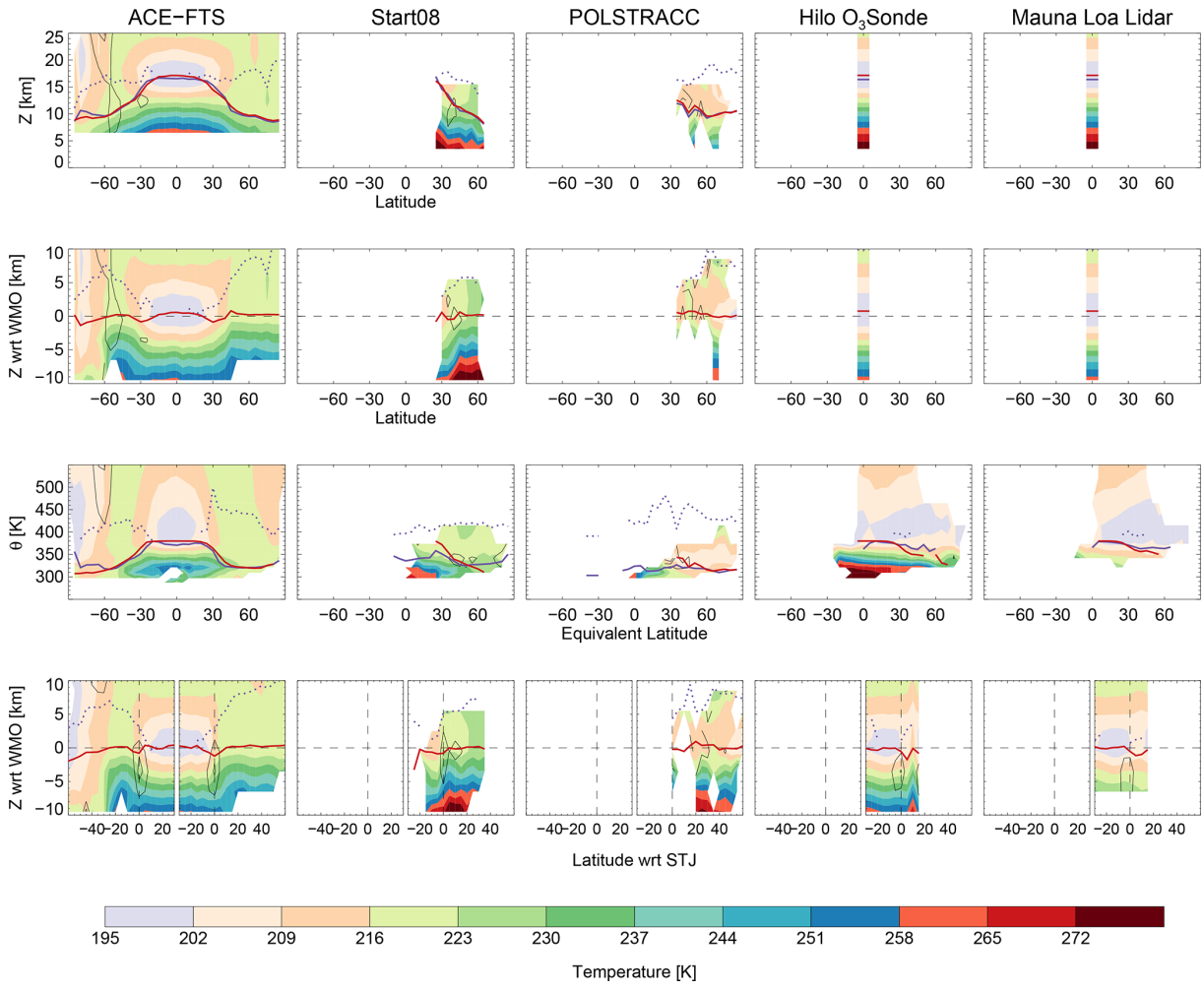

Figure A2. MERRA-2 temperature sampled at ACE-FTS, START08POLSTRACC, Hilo ozonesonde, and Mauna Loa lidar measurements in different coordinate systems. ACE-FTS panel displays 2018 data, Hilo ozonesonde and Lauder lidar show data post 2005, and START08 and POLSTRACC display all their available data. Red lines show the 4.5 PVU dynamical tropopause and purple lines the WMO (thermal) tropopause (dotted purple lines show the secondary thermal tropopause). The black contours show wind speed values of 30, 40, and 50 m s^{-1}. Note that differences in their representation in comparison with MLS suggest sampling biases. Datasets were binned on a 5° horizontal grid and a 5 km or 5 K grid.

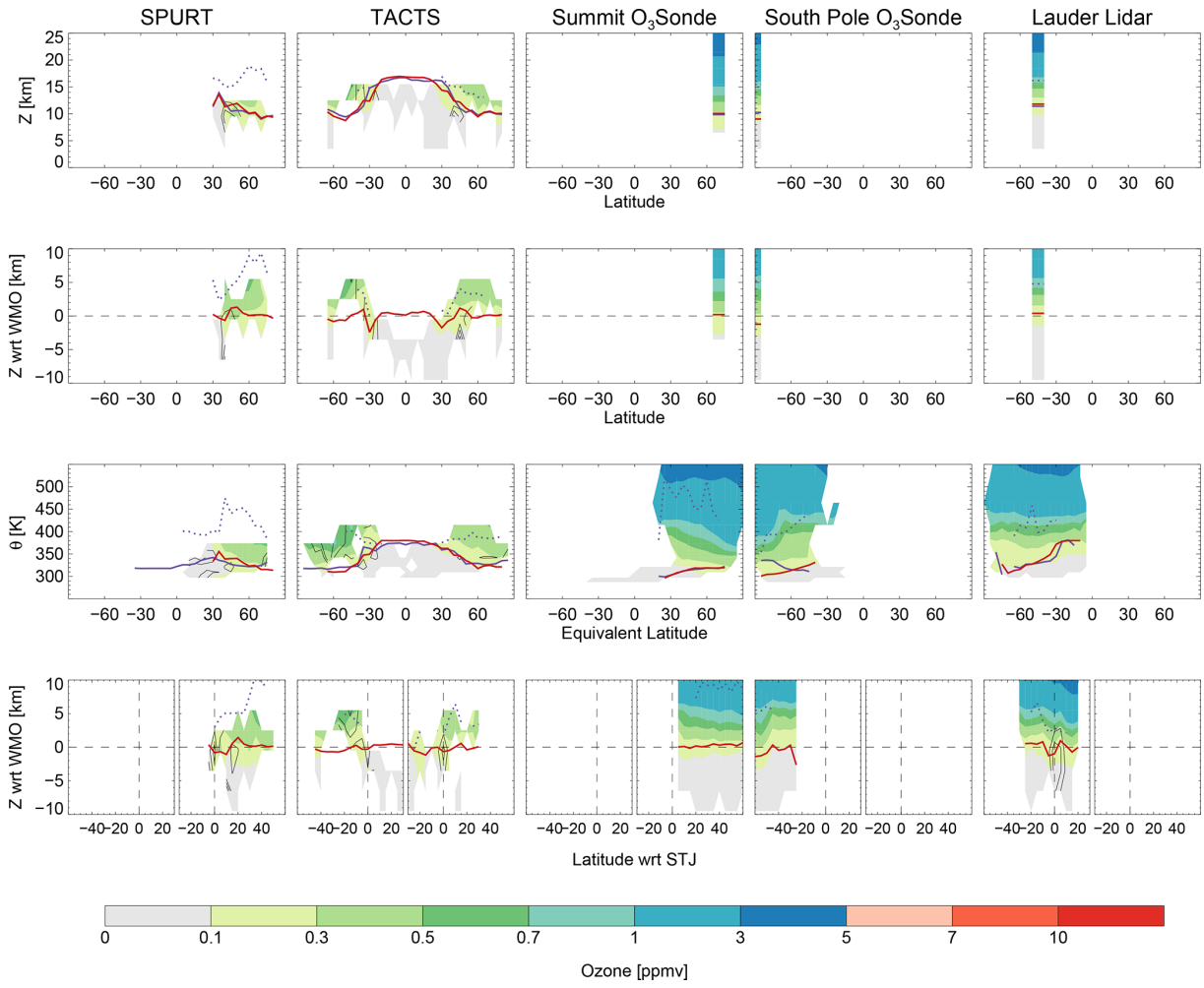

Figure A3. Climatological SPURT, TACTS, Summit and South Pole ozonesondes, and Lauder lidar ozone data in different coordinate systems. Summit, South Pole ozonesonde, and Lauder lidar show data post 2005, and SPURT and TACTS display all their available data. Red lines show the 4.5 PVU dynamical tropopause and purple lines the WMO (thermal) tropopause (dotted purple lines show the secondary thermal tropopause). The black contours show wind speed values of 30, 40, and 50 $\mathrm{m\,s^{-1}}$. Note that differences in their representation in comparison with MLS suggest sampling biases. Datasets were binned on a 5° horizontal grid and a 5 km or 5 K grid.

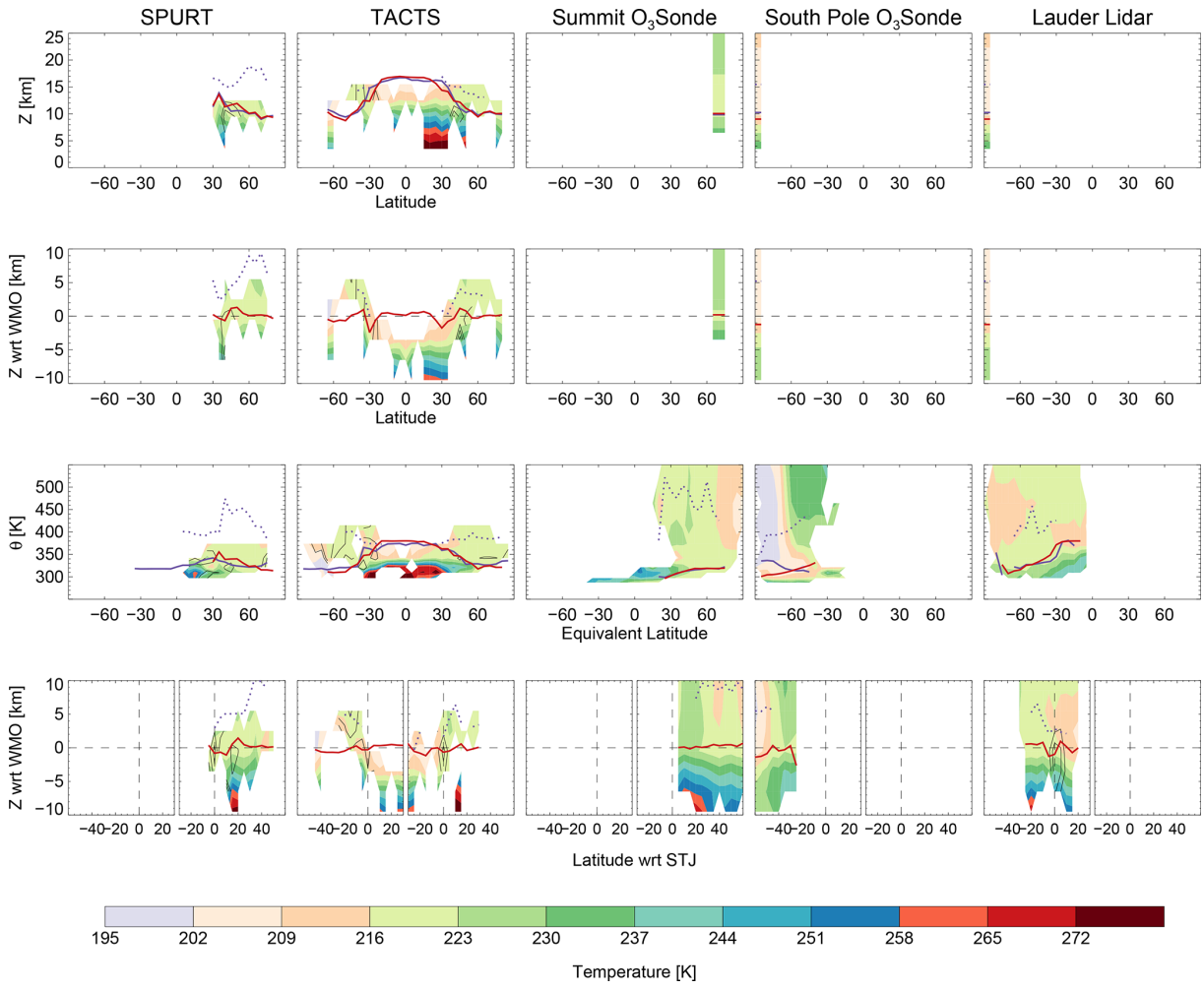

Figure A4. MERRA-2 temperature sampled at SPURT, TACTS Summit, and South Pole ozonesondes, and Lauder lidar measurements in different coordinate systems. Summit and South Pole ozonesonde and Lauder lidar show data post 2005, and SPURT and TACTS display all their available data. Red lines show the 4.5 PVU dynamical tropopause and purple lines the WMO (thermal) tropopause (dotted purple lines show the secondary thermal tropopause). The black contours show wind speed values of 30, 40, and 50 m s^{-1}. Note that differences in their representation in comparison with MLS suggest sampling biases. Datasets were binned on a 5° horizontal grid and a 5 km or 5 K grid.

Data availability. The ozone datasets used are available as follows:

- ozonesondes – https://gml.noaa.gov/aftp/data/ozwv/Ozonesonde/ (Global Monitoring Laboratory, 2023),
- lidar – https://www-air.larc.nasa.gov/missions/ndacc/data.html (Network for the Detection of Atmospheric Composition Change, 2023),
- SPURT – through contact with Peter Hoor (hoor@uni-mainz.de) or Daniel Kunkel (dkunkel@uni-mainz.de),
- WISE – https://halo-db.pa.op.dlr.de/ (German Aerospace Center, 2023a),
- START08 – https://doi.org/10.5065/D62V2DG5 (UCAR/NCAR, 2023),
- TACTS/ESMVal – https://halo-db.pa.op.dlr.de/ (German Aerospace Center, 2023b),
- PGS – https://halo-db.pa.op.dlr.de/ (German Aerospace Center, 2023c),
- CARIBIC-1 and 2 – https://www.caribic-atmospheric.com/Data.php (IAGOS, 2023),
- ACE-FTS – http://www.ace.uwaterloo.ca/data.php (University of Waterloo, 2023),
- ACE-FTS quality information – https://doi.org/10.5683/SP2/BC4ATC (Sheese and Walker, 2020),
- Aura MLS – https://doi.org/10.5067/Aura/MLS/DATA2516 (Schwartz et al., 2020), and,
- SAGEIII/ISS – https://asdc.larc.nasa.gov/ (login required, Atmospheric Science Data Center, 2023)

For the dynamical diagnostics please contact Gloria L. Manney (manney@nwra.com) or Luis F. Millán (lmillan@jpl.nasa.gov).

Author contributions. GLM wrote most of the core JETPAC software. LFM generalized the code to cope with several types of datasets. LMV wrote the paper. All the co-authors commented on and edited the manuscript. IP provided the ozonesonde datasets; TL provided the lidar datasets; PH and DK provided the SPURT, WISE, TACTS/ESMVal, and PGS datasets; and AZ and HB provided the CARIBIC-1 and CARIBIC-2 datasets.

Competing interests. The contact author has declared that none of the authors has any competing interests.

Disclaimer. Publisher's note: Copernicus Publications remains neutral with regard to jurisdictional claims in published maps and institutional affiliations.

Acknowledgements. Luis F. Millán's and Thierry Leblanc's research was carried out at the Jet Propulsion Laboratory, California Institute of Technology, under a contract with the National Aeronautics and Space Administration (80NM0018D0004). Gloria L. Manney was supported by subcontracts from JPL through the Microwave Limb Sounder (MLS) project and the SAGEIII/ISS project. Peter Hoor and Daniel Kunkel acknowledge support by the German Science Foundation (DFG) through TRR 301 (project 428312742). Irina Petropavlovskikh's research was supported by the NOAA Cooperative Agreement with CIRES, NA17OAR4320101. We thank the JPL MLS team (especially Brian Knosp and Ryan Fuller) for data management and processing support and William Daffer for work on early development of JETPAC. MERRA-2 is an official product of the Global Modeling and Assimilation Office at NASA GSFC, funded by Modeling Analysis and Prediction. The Atmospheric Chemistry Experiment is a Canadian-led mission, primarily supported by the CSA.

Financial support. This research has been supported by the National Aeronautics and Space Administration (grant no. 80NM0018D0004), the Jet Propulsion Laboratory (Microwave Limb Sounder (MLS) project and SAGEIII/ISS project), the German Science Foundation (DFG) through TRR 301 (project 428312742), and the NOAA Cooperative Agreement with CIRES (grant no. NA17OAR4320101).

Review statement. This paper was edited by Mark Weber and reviewed by two anonymous referees.

References

Albers, J. R., Perlwitz, J., Butler, A. H., Birner, T., Kiladis, G. N., Lawrence, Z. D., Manney, G. L., Langford, A. O., and Dias, J.: Mechanisms Governing Interannual Variability of Stratosphere-to-Troposphere Ozone Transport, J. Geophys. Res.-Atmos., 123, 234–260, https://doi.org/10.1002/2017jd026890, 2018.

Añel, J. A., Allen, D. R., Sáenz, G., Gimeno, L., and de la Torre, L.: Equivalent Latitude Computation Using Regions of Interest (ROI), PLoS ONE, 8, e72970, https://doi.org/10.1371/journal.pone.0072970, 2013.

Atmospheric Science Data Center: SAGEIII/ISS, Atmospheric Science Data Center, https://asdc.larc.nasa.gov/, last access: 1 February 2023.

Ball, W. T., Alsing, J., Mortlock, D. J., Staehelin, J., Haigh, J. D., Peter, T., Tummon, F., Stübi, R., Stenke, A., Anderson, J., Bourassa, A., Davis, S. M., Degenstein, D., Frith, S., Froidevaux, L., Roth, C., Sofieva, V., Wang, R., Wild, J., Yu, P., Ziemke, J. R., and Rozanov, E. V.: Evidence for a continuous decline in lower stratospheric ozone offsetting ozone layer recovery, Atmos. Chem. Phys., 18, 1379–1394, https://doi.org/10.5194/acp-18-1379-2018, 2018.

Ball, W. T., Alsing, J., Staehelin, J., Davis, S. M., Froidevaux, L., and Peter, T.: Stratospheric ozone trends for 1985–2018: sensitivity to recent large variability, Atmos. Chem. Phys., 19, 12731–12748, https://doi.org/10.5194/acp-19-12731-2019, 2019.

Barnes, E. A. and Screen, J. A.: The impact of Arctic warming on the midlatitude jet-stream: Can it? Has it? Will it?, WIRES Clim. Change, 6, 277–286, 2015.

Bernath, P. F., McElroy, C. T., Abrams, M. C., Boone, C. D., Butler, M., Camy-Peyret, C., Carleer, M., Clerbaux, C., Coheur, P.-F., Colin, R., DeCola, P., DeMazière, M., Drummond, J. R., Dufour, D., Evans, W. F. J., Fast, H., Fussen, D., Gilbert, K., Jen-

nings, D. E., Llewellyn, E. J., Lowe, R. P., Mahieu, E., McConnell, J. C., McHugh, M., McLeod, S. D., Michaud, R., Midwinter, C., Nassar, R., Nichitiu, F., Nowlan, C., Rinsland, C. P., Rochon, Y. J., Rowlands, N., Semeniuk, K., Simon, P., Skelton, R., Sloan, J. J., Soucy, M.-A., Strong, K., Tremblay, P., Turnbull, D., Walker, K. A., Walkty, I., Wardle, D. A., Wehrle, V., Zander, R., and Zou, J.: Atmospheric Chemistry Experiment (ACE): Mission overview, Geophys. Res. Lett., 32, L15S01, https://doi.org/10.1029/2005gl022386, 2005.

Birner, T., Dörnbrack, A., and Schumann, U.: How sharp is the tropopause at midlatitudes?, Geophys. Res. Lett., 29, 45-1–45-4, https://doi.org/10.1029/2002gl015142, 2002.

Birner, T., Sankey, D., and Shepherd, T. G.: The tropopause inversion layer in models and analyses, Geophys. Res. Lett., 33, L14804, https://doi.org/10.1029/2006gl026549, 2006.

Bloom, S. C., Takacs, L. L., da Silva, A. M., and Ledvina, D.: Data Assimilation Using Incremental Analysis Updates, Mon. Weather Rev., 124, 1256–1271, https://doi.org/10.1175/1520-0493(1996)124<1256:DAUIAU>2.0.CO;2, 1996.

Bognar, K., Zhao, X., Strong, K., Boone, C., Bourassa, A., Degenstein, D., Drummond, J., Duff, A., Goutail, F., Griffin, D., Jeffery, P., Lutsch, E., Manney, G., McElroy, C., McLinden, C., Millán, L., Pazmino, A., Sioris, C., Walker, K., and Zou, J.: Updated validation of ACE and OSIRIS ozone and NO_2 measurements in the Arctic using ground-based instruments at Eureka, Canada, J. Quant. Spectrosc. Ra., 238, 106571, https://doi.org/10.1016/j.jqsrt.2019.07.014, 2019.

Bognar, K., Tegtmeier, S., Bourassa, A., Roth, C., Warnock, T., Zawada, D., and Degenstein, D.: Stratospheric ozone trends for 1984–2021 in the SAGE II–OSIRIS–SAGE II-I/ISS composite dataset, Atmos. Chem. Phys., 22, 9553–9569, https://doi.org/10.5194/acp-22-9553-2022, 2022.

Bönisch, H., Engel, A., Curtius, J., Birner, Th., and Hoor, P.: Quantifying transport into the lowermost stratosphere using simultaneous in-situ measurements of SF_6 and CO_2, Atmos. Chem. Phys., 9, 5905–5919, https://doi.org/10.5194/acp-9-5905-2009, 2009.

Brenninkmeijer, C. A. M., Crutzen, P. J., Fischer, H., Güsten, H., Hans, W., Heinrich, G., Heintzenberg, J., Hermann, M., Immelmann, T., Kersting, D., Maiss, M., Nolle, M., Pitscheider, A., Pohlkamp, H., Scharffe, D., Specht, K., and Wiedensohler, A.: CARIBIC – Civil Aircraft for Global Measurement of Trace Gases and Aerosols in the Tropopause Region, J. Atmos. Ocean. Tech., 16, 1373–1383, https://doi.org/10.1175/1520-0426(1999)016<1373:ccafgm>2.0.co;2, 1999.

Brenninkmeijer, C. A. M., Crutzen, P., Boumard, F., Dauer, T., Dix, B., Ebinghaus, R., Filippi, D., Fischer, H., Franke, H., Frieß, U., Heintzenberg, J., Helleis, F., Hermann, M., Kock, H. H., Koeppel, C., Lelieveld, J., Leuenberger, M., Martinsson, B. G., Miemczyk, S., Moret, H. P., Nguyen, H. N., Nyfeler, P., Oram, D., O'Sullivan, D., Penkett, S., Platt, U., Pupek, M., Ramonet, M., Randa, B., Reichelt, M., Rhee, T. S., Rohwer, J., Rosenfeld, K., Scharffe, D., Schlager, H., Schumann, U., Slemr, F., Sprung, D., Stock, P., Thaler, R., Valentino, F., van Velthoven, P., Waibel, A., Wandel, A., Waschitschek, K., Wiedensohler, A., Xueref-Remy, I., Zahn, A., Zech, U., and Ziereis, H.: Civil Aircraft for the regular investigation of the atmosphere based on an instrumented container: The new CARIBIC system, Atmos. Chem. Phys., 7, 4953–4976, https://doi.org/10.5194/acp-7-4953-2007, 2007.

Brunner, D., Staehelin, J., Maeder, J. A., Wohltmann, I., and Bodeker, G. E.: Variability and trends in total and vertically resolved stratospheric ozone based on the CATO ozone data set, Atmos. Chem. Phys., 6, 4985–5008, https://doi.org/10.5194/acp-6-4985-2006, 2006.

Butchart, N. and Remsberg, E.: The Area of the Stratospheric Polar Vortex as a Diagnostic for Tracer Transport on an Isentropic Surface, J. Atmos. Sci., 43, 1319–1339, https://doi.org/10.1175/1520-0469(1986)043<1319:TAOTSP>2.0.CO;2, 1986.

Chang, K.-L., Cooper, O. R., Gaudel, A., Petropavlovskikh, I., and Thouret, V.: Statistical regularization for trend detection: an integrated approach for detecting long-term trends from sparse tropospheric ozone profiles, Atmos. Chem. Phys., 20, 9915–9938, https://doi.org/10.5194/acp-20-9915-2020, 2020.

Chiou, E.-W., Thomason, L. W., Burton, S. P., and Michelsen, H. A.: Assessment of the SAGE II version 6.2 water vapor data set through intercomparison with ATMOS/ATLAS-3 measurements, Geophys. Res. Lett., 31, L14101, https://doi.org/10.1029/2004gl020071, 2004.

Chipperfield, M. P., Dhomse, S., Hossaini, R., Feng, W., Santee, M. L., Weber, M., Burrows, J. P., Wild, J. D., Loyola, D., and Coldewey-Egbers, M.: On the Cause of Recent Variations in Lower Stratospheric Ozone, Geophys. Res. Lett., 45, 5718–5726, https://doi.org/10.1029/2018gl078071, 2018.

Cohen, Y., Petetin, H., Thouret, V., Marécal, V., Josse, B., Clark, H., Sauvage, B., Fontaine, A., Athier, G., Blot, R., Boulanger, D., Cousin, J.-M., and Nédélec, P.: Climatology and long-term evolution of ozone and carbon monoxide in the upper troposphere–lower stratosphere (UTLS) at northern midlatitudes, as seen by IAGOS from 1995 to 2013, Atmos. Chem. Phys., 18, 5415–5453, https://doi.org/10.5194/acp-18-5415-2018, 2018.

Cohen, Y., Marécal, V., Josse, B., and Thouret, V.: Interpol-IAGOS: a new method for assessing long-term chemistry–climate simulations in the UTLS based on IAGOS data, and its application to the MOCAGE CCMI REF-C1SD simulation, Geosci. Model Dev., 14, 2659–2689, https://doi.org/10.5194/gmd-14-2659-2021, 2021.

Cooper, O. R., Parrish, D. D., Stohl, A., Trainer, M., Nédélec, P., Thouret, V., Cammas, J. P., Oltmans, S. J., Johnson, B. J., Tarasick, D., Leblanc, T., McDermid, I. S., Jaffe, D., Gao, R., Stith, J., Ryerson, T., Aikin, K., Campos, T., Weinheimer, A., and Avery, M. A.: Increasing springtime ozone mixing ratios in the free troposphere over western North America, Nature, 463, 344–348, https://doi.org/10.1038/nature08708, 2010.

Davis, S. M., Hegglin, M. I., Fujiwara, M., Dragani, R., Harada, Y., Kobayashi, C., Long, C., Manney, G. L., Nash, E. R., Potter, G. L., Tegtmeier, S., Wang, T., Wargan, K., and Wright, J. S.: Assessment of upper tropospheric and stratospheric water vapor and ozone in reanalyses as part of S-RIP, Atmos. Chem. Phys., 17, 12743–12778, https://doi.org/10.5194/acp-17-12743-2017, 2017.

De Mazière, M., Thompson, A. M., Kurylo, M. J., Wild, J. D., Bernhard, G., Blumenstock, T., Braathen, G. O., Hannigan, J. W., Lambert, J.-C., Leblanc, T., McGee, T. J., Nedoluha, G., Petropavlovskikh, I., Seckmeyer, G., Simon, P. C., Steinbrecht, W., and Strahan, S. E.: The Network for the Detection of Atmospheric Composition Change (NDACC): history,

status and perspectives, Atmos. Chem. Phys., 18, 4935–4964, https://doi.org/10.5194/acp-18-4935-2018, 2018.

Dupuy, E., Walker, K. A., Kar, J., Boone, C. D., McElroy, C. T., Bernath, P. F., Drummond, J. R., Skelton, R., McLeod, S. D., Hughes, R. C., Nowlan, C. R., Dufour, D. G., Zou, J., Nichitiu, F., Strong, K., Baron, P., Bevilacqua, R. M., Blumenstock, T., Bodeker, G. E., Borsdorff, T., Bourassa, A. E., Bovensmann, H., Boyd, I. S., Bracher, A., Brogniez, C., Burrows, J. P., Catoire, V., Ceccherini, S., Chabrillat, S., Christensen, T., Coffey, M. T., Cortesi, U., Davies, J., De Clercq, C., Degenstein, D. A., De Mazière, M., Demoulin, P., Dodion, J., Firanski, B., Fischer, H., Forbes, G., Froidevaux, L., Fussen, D., Gerard, P., Godin-Beekmann, S., Goutail, F., Granville, J., Griffith, D., Haley, C. S., Hannigan, J. W., Höpfner, M., Jin, J. J., Jones, A., Jones, N. B., Jucks, K., Kagawa, A., Kasai, Y., Kerzenmacher, T. E., Kleinböhl, A., Klekociuk, A. R., Kramer, I., Küllmann, H., Kuttippurath, J., Kyrölä, E., Lambert, J.-C., Livesey, N. J., Llewellyn, E. J., Lloyd, N. D., Mahieu, E., Manney, G. L., Marshall, B. T., McConnell, J. C., McCormick, M. P., McDermid, I. S., McHugh, M., McLinden, C. A., Mellqvist, J., Mizutani, K., Murayama, Y., Murtagh, D. P., Oelhaf, H., Parrish, A., Petelina, S. V., Piccolo, C., Pommereau, J.-P., Randall, C. E., Robert, C., Roth, C., Schneider, M., Senten, C., Steck, T., Strandberg, A., Strawbridge, K. B., Sussmann, R., Swart, D. P. J., Tarasick, D. W., Taylor, J. R., Tétard, C., Thomason, L. W., Thompson, A. M., Tully, M. B., Urban, J., Vanhellemont, F., Vigouroux, C., von Clarmann, T., von der Gathen, P., von Savigny, C., Waters, J. W., Witte, J. C., Wolff, M., and Zawodny, J. M.: Validation of ozone measurements from the Atmospheric Chemistry Experiment (ACE), Atmos. Chem. Phys., 9, 287–343, https://doi.org/10.5194/acp-9-287-2009, 2009.

Engel, A., Bönisch, H., Brunner, D., Fischer, H., Franke, H., Günther, G., Gurk, C., Hegglin, M., Hoor, P., Königstedt, R., Krebsbach, M., Maser, R., Parchatka, U., Peter, T., Schell, D., Schiller, C., Schmidt, U., Spelten, N., Szabo, T., Weers, U., Wernli, H., Wetter, T., and Wirth, V.: Highly resolved observations of trace gases in the lowermost stratosphere and upper troposphere from the Spurt project: an overview, Atmos. Chem. Phys., 6, 283–301, https://doi.org/10.5194/acp-6-283-2006, 2006.

Forster, P. M. d. F. and Shine, K. P.: Radiative forcing and temperature trends from stratospheric ozone changes, J. Geophys. Res.-Atmos., 102, 10841–10855, https://doi.org/10.1029/96jd03510, 1997.

Francis, J. A.: Why Are Arctic Linkages to Extreme Weather Still up in the Air?, B. Am. Meteorol. Soc., 98, 2551–2557, https://doi.org/10.1175/BAMS-D-17-0006.1, 2017.

Froidevaux, L., Jiang, Y. B., Lambert, A., Livesey, N. J., Read, W. G., Waters, J. W., Browell, E. V., Hair, J. W., Avery, M. A., McGee, T. J., Twigg, L. W., Sumnicht, G. K., Jucks, K. W., Margitan, J. J., Sen, B., Stachnik, R. A., Toon, G. C., Bernath, P. F., Boone, C. D., Walker, K. A., Filipiak, M. J., Harwood, R. S., Fuller, R. A., Manney, G. L., Schwartz, M. J., Daffer, W. H., Drouin, B. J., Cofield, R. E., Cuddy, D. T., Jarnot, R. F., Knosp, B. W., Perun, V. S., Snyder, W. V., Stek, P. C., Thurstans, R. P., and Wagner, P. A.: Validation of Aura Microwave Limb Sounder stratospheric ozone measurements, J. Geophys. Res.-Atmos., 113, D15S20, https://doi.org/10.1029/2007JD008771, 2008.

Fujiwara, M., Wright, J. S., Manney, G. L., Gray, L. J., Anstey, J., Birner, T., Davis, S., Gerber, E. P., Harvey, V. L., Hegglin, M. I., Homeyer, C. R., Knox, J. A., Krüger, K., Lambert, A., Long, C. S., Martineau, P., Molod, A., Monge-Sanz, B. M., Santee, M. L., Tegtmeier, S., Chabrillat, S., Tan, D. G. H., Jackson, D. R., Polavarapu, S., Compo, G. P., Dragani, R., Ebisuzaki, W., Harada, Y., Kobayashi, C., McCarty, W., Onogi, K., Pawson, S., Simmons, A., Wargan, K., Whitaker, J. S., and Zou, C.-Z.: Introduction to the SPARC Reanalysis Intercomparison Project (S-RIP) and overview of the reanalysis systems, Atmos. Chem. Phys., 17, 1417–1452, https://doi.org/10.5194/acp-17-1417-2017, 2017.

Fujiwara, M., Manney, G., Gray, L., and Wright, J.: SPARC Report No. 10, SPARC Reanalysis Intercomparison Project (S-RIP) Final Report, WCRP Report 6/2021, https://doi.org/10.17874/800DEE57D13, 2022.

Gelaro, R., McCarty, W., Suárez, M. J., Todling, R., Molod, A., Takacs, L., Randles, C. A., Darmenov, A., Bosilovich, M. G., Reichle, R., Wargan, K., Coy, L., Cullather, R., Draper, C., Akella, S., Buchard, V., Conaty, A., da Silva, A. M., Gu, W., Kim, G.-K., Koster, R., Lucchesi, R., Merkova, D., Nielsen, J. E., Partyka, G., Pawson, S., Putman, W., Rienecker, M., Schubert, S. D., Sienkiewicz, M., and Zhao, B.: The Modern-Era Retrospective Analysis for Research and Applications, Version 2 (MERRA-2), J. Climate, 30, 5419–5454, https://doi.org/10.1175/jcli-d-16-0758.1, 2017.

German Aerospace Center: WISE, HALO database, https://halo-db.pa.op.dlr.de/, last access: 1 February 2023a.

German Aerospace Center: TACTS/ESMVal, HALO database, https://halo-db.pa.op.dlr.de/, last access: 1 February 2023b.

German Aerospace Center: PGS, HALO database, https://halo-db.pa.op.dlr.de/, last access: 1 February 2023c.

Gettelman, A. and Wang, T.: Structural diagnostics of the tropopause inversion layer and its evolution, J. Geophys. Res.-Atmos., 120, 46–62, https://doi.org/10.1002/2014jd021846, 2015.

Gettelman, A., Hoor, P., Pan, L. L., Randel, W. J., Hegglin, M. I., and Birner, T.: The Extratropical Upper Troposphere and Lower Stratosphere, Rev. Geophys., 49, RG3003, https://doi.org/10.1029/2011rg000355, 2011.

Gijsel, J. A. E. V., Swart, D. P. J., Baray, J.-L., Claude, H., Fehr, T., Gathen, P. V. D., Godin-Beekmann, S., Hansen, G. H., Leblanc, T., McDermid, I. S., Meijer, Y. J., Nakane, H., Quel, E. J., Steinbrecht, W., Strawbridge, K. B., Tatarov, B., and Wolfram, E. A.: Global validation of ENVISAT ozone profiles using lidar measurements, Int. J. Remote Sens., 30, 3987–3994, https://doi.org/10.1080/01431160902821825, 2009.

Global Monitoring Laboratory: Ozonesondes, NOAA [data set], https://gml.noaa.gov/aftp/data/ozwv/Ozonesonde/, last access: 1 February 2023.

Godin-Beekmann, S., Porteneuve, J., and Garnier, A.: Systematic DIAL lidar monitoring of the stratospheric ozone vertical distribution at Observatoire de Haute-Provence (43.92° N, 5.71° E), J. Environ. Monitor., 5, 57–67, https://doi.org/10.1039/b205880d, 2002.

Godin-Beekmann, S., Azouz, N., Sofieva, V. F., Hubert, D., Petropavlovskikh, I., Effertz, P., Ancellet, G., Degenstein, D. A., Zawada, D., Froidevaux, L., Frith, S., Wild, J., Davis, S., Steinbrecht, W., Leblanc, T., Querel, R., Tourpali, K., Damadeo, R., Maillard Barras, E., Stübi, R., Vigouroux, C., Arosio, C., Nedoluha, G., Boyd, I., Van Malderen, R., Mahieu, E., Smale,

D., and Sussmann, R.: Updated trends of the stratospheric ozone vertical distribution in the 60° S–60° N latitude range based on the LOTUS regression model , Atmos. Chem. Phys., 22, 11657–11673, https://doi.org/10.5194/acp-22-11657-2022, 2022.

Griffin, D., Walker, K. A., Conway, S., Kolonjari, F., Strong, K., Batchelor, R., Boone, C. D., Dan, L., Drummond, J. R., Fogal, P. F., Fu, D., Lindenmaier, R., Manney, G. L., and Weaver, D.: Multi-year comparisons of ground-based and space-borne Fourier transform spectrometers in the high Arctic between 2006 and 2013, Atmos. Meas. Tech., 10, 3273–3294, https://doi.org/10.5194/amt-10-3273-2017, 2017.

Grise, K. M., Thompson, D. W. J., and Birner, T.: A Global Survey of Static Stability in the Stratosphere and Upper Troposphere, J. Climate, 23, 2275–2292, https://doi.org/10.1175/2009jcli3369.1, 2010.

Harris, N. R. P., Hassler, B., Tummon, F., Bodeker, G. E., Hubert, D., Petropavlovskikh, I., Steinbrecht, W., Anderson, J., Bhartia, P. K., Boone, C. D., Bourassa, A., Davis, S. M., Degenstein, D., Delcloo, A., Frith, S. M., Froidevaux, L., Godin-Beekmann, S., Jones, N., Kurylo, M. J., Kyrölä, E., Laine, M., Leblanc, S. T., Lambert, J.-C., Liley, B., Mahieu, E., Maycock, A., de Mazière, M., Parrish, A., Querel, R., Rosenlof, K. H., Roth, C., Sioris, C., Staehelin, J., Stolarski, R. S., Stübi, R., Tamminen, J., Vigouroux, C., Walker, K. A., Wang, H. J., Wild, J., and Zawodny, J. M.: Past changes in the vertical distribution of ozone – Part 3: Analysis and interpretation of trends, Atmos. Chem. Phys., 15, 9965–9982, https://doi.org/10.5194/acp-15-9965-2015, 2015.

Hegglin, M. I. and Tegtmeier, S.: The SPARC Data Initiative: Assessment of stratospheric trace gas and aerosol climatologies from satellite limb sounders, ETH-Zürich, Tech. rep., https://doi.org/10.3929/ETHZ-A-010863911, 2017.

Hegglin, M. I., Brunner, D., Peter, T., Hoor, P., Fischer, H., Staehelin, J., Krebsbach, M., Schiller, C., Parchatka, U., and Weers, U.: Measurements of NO, NO_y, N_2O, and O_3 during SPURT: implications for transport and chemistry in the lowermost stratosphere, Atmos. Chem. Phys., 6, 1331–1350, https://doi.org/10.5194/acp-6-1331-2006, 2006.

Hegglin, M. I., Boone, C. D., Manney, G. L., Shepherd, T. G., Walker, K. A., Bernath, P. F., Daffer, W. H., Hoor, P., and Schiller, C.: Validation of ACE-FTS satellite data in the upper troposphere/lower stratosphere (UTLS) using non-coincident measurements, Atmos. Chem. Phys., 8, 1483–1499, https://doi.org/10.5194/acp-8-1483-2008, 2008.

Hegglin, M. I., Boone, C. D., Manney, G. L., and Walker, K. A.: A global view of the extratropical tropopause transition layer from Atmospheric Chemistry Experiment Fourier Transform Spectrometer O_3, H_2O, and CO, J. Geophys. Res.-Atmos., 114, D00B11, https://doi.org/10.1029/2008JD009984, 2009.

Hegglin, M. I., Tegtmeier, S., Anderson, J., Bourassa, A. E., Brohede, S., Degenstein, D., Froidevaux, L., Funke, B., Gille, J., Kasai, Y., Kyrölä, E. T., Lumpe, J., Murtagh, D., Neu, J. L., Pérot, K., Remsberg, E. E., Rozanov, A., Toohey, M., Urban, J., von Clarmann, T., Walker, K. A., Wang, H.-J., Arosio, C., Damadeo, R., Fuller, R. A., Lingenfelser, G., McLinden, C., Pendlebury, D., Roth, C., Ryan, N. J., Sioris, C., Smith, L., and Weigel, K.: Overview and update of the SPARC Data Initiative: comparison of stratospheric composition measurements from satellite limb sounders, Earth Syst. Sci. Data, 13, 1855–1903, https://doi.org/10.5194/essd-13-1855-2021, 2021.

Highwood, E. J., Hoskins, B. J., and Berrisford, P.: Properties of the arctic tropopause, Q. J. Roy. Meteor. Soc., 126, 1515–1532, https://doi.org/10.1002/qj.49712656515, 2000.

Holton, J. R., Haynes, P. H., McIntyre, M. E., Douglass, A. R., Rood, R. B., and Pfister, L.: Stratosphere-troposphere exchange, Rev. Geophys., 33, 403–439, https://doi.org/10.1029/95rg02097, 1995.

Homeyer, C. R., Bowman, K. P., and Pan, L. L.: Extratropical tropopause transition layer characteristics from high-resolution sounding data, J. Geophys. Res.-Atmos., 115, D13108, https://doi.org/10.1029/2009JD013664, 2010.

Homeyer, C. R., Manney, G. L., Millán, L. F., Boothe, A. C., Xian, T., Olsen, M. A., Schwartz, M. J., Lawrence, Z. D., and Wargan, K.: Extratropical Upper Troposphere and Lower Stratosphere (ExUTLS), Chap. 7 of SPARC Reanalysis Intercomparison Project (S-RIP) Final Report, edited by: Fujiwara, M., Manney, G. L., Gray, L. J., and Wright, J. S., SPARC Report No. 10, WCRP-6/2021, https://doi.org/10.17874/800dee57d13, 2022.

Hoor, P., Gurk, C., Brunner, D., Hegglin, M. I., Wernli, H., and Fischer, H.: Seasonality and extent of extratropical TST derived from in-situ CO measurements during SPURT, Atmos. Chem. Phys., 4, 1427–1442, https://doi.org/10.5194/acp-4-1427-2004, 2004.

Hoor, P., Wernli, H., Hegglin, M. I., and Bönisch, H.: Transport timescales and tracer properties in the extratropical UTLS, Atmos. Chem. Phys., 10, 7929–7944, https://doi.org/10.5194/acp-10-7929-2010, 2010.

Hoor, P., Petropavlovskikh, I., Millán, L., and Kunkel, D.: Report on the second SPARC OCTAV-UTLS meeting, Mainz, Germany, 7–9 November 2010, SPARC, https://www.sparc-climate.org/wp-content/uploads/sites/5/2019/07/SPARCnewsletter_July2019_WEB.pdf (last access: 1 February 2023), 2019.

Hoskins, B. J., McIntyre, M. E., and Robertson, A. W.: On the use and significance of isentropic potential vorticity maps, Q. J. Roy. Meteorol. Soc., 111, 877–946, https://doi.org/10.1002/qj.49711147002, 1985.

Hubert, D., Lambert, J.-C., Verhoelst, T., Granville, J., Keppens, A., Baray, J.-L., Bourassa, A. E., Cortesi, U., Degenstein, D. A., Froidevaux, L., Godin-Beekmann, S., Hoppel, K. W., Johnson, B. J., Kyrölä, E., Leblanc, T., Lichtenberg, G., Marchand, M., McElroy, C. T., Murtagh, D., Nakane, H., Portafaix, T., Querel, R., Russell III, J. M., Salvador, J., Smit, H. G. J., Stebel, K., Steinbrecht, W., Strawbridge, K. B., Stübi, R., Swart, D. P. J., Taha, G., Tarasick, D. W., Thompson, A. M., Urban, J., van Gijsel, J. A. E., Van Malderen, R., von der Gathen, P., Walker, K. A., Wolfram, E., and Zawodny, J. M.: Ground-based assessment of the bias and long-term stability of 14 limb and occultation ozone profile data records, Atmos. Meas. Tech., 9, 2497–2534, https://doi.org/10.5194/amt-9-2497-2016, 2016.

IAGOS: CARIBIC-1 and 2, IAGOS [data set], https://www.caribic-atmospheric.com/Data.php, last access: 1 February 2023.

Jeffery, P. S., Walker, K. A., Sioris, C. E., Boone, C. D., Degenstein, D., Manney, G. L., McElroy, C. T., Millán, L., Plummer, D. A., Ryan, N. J., Sheese, P. E., and Zou, J.: Water vapour and ozone in the upper troposphere–lower stratosphere: global climatologies from three Canadian limb-viewing instruments, Atmos. Chem.

Phys., 22, 14709–14734, https://doi.org/10.5194/acp-22-14709-2022, 2022.

Jiang, Y. B., Froidevaux, L., Lambert, A., Livesey, N. J., Read, W. G., Waters, J. W., Bojkov, B., Leblanc, T., McDermid, I. S., Godin-Beekmann, S., Filipiak, M. J., Harwood, R. S., Fuller, R. A., Daffer, W. H., Drouin, B. J., Cofield, R. E., Cuddy, D. T., Jarnot, R. F., Knosp, B. W., Perun, V. S., Schwartz, M. J., Snyder, W. V., Stek, P. C., Thurstans, R. P., Wagner, P. A., Allaart, M., Andersen, S. B., Bodeker, G., Calpini, B., Claude, H., Coetzee, G., Davies, J., De Backer, H., Dier, H., Fujiwara, M., Johnson, B., Kelder, H., Leme, N. P., König-Langlo, G., Kyro, E., Laneve, G., Fook, L. S., Merrill, J., Morris, G., Newchurch, M., Oltmans, S., Parrondos, M. C., Posny, F., Schmidlin, F., Skrivankova, P., Stubi, R., Tarasick, D., Thompson, A., Thouret, V., Viatte, P., Vömel, H., von Der Gathen, P., Yela, M., and Zablocki, G.: Validation of Aura Microwave Limb Sounder Ozone by ozonesonde and lidar measurements, J. Geophys. Res.-Atmos., 112, D24S34, https://doi.org/10.1029/2007JD008776, 2007.

Jin, J. J., Livesey, N. J., Manney, G. L., Jiang, J. H., Schwartz, M. J., and Daffer, W. H.: Chemical discontinuity at the extratropical tropopause and isentropic stratosphere-troposphere exchange pathways diagnosed using Aura MLS data, J. Geophys. Res.-Atmos., 118, 3832–3847, https://doi.org/10.1002/jgrd.50291, 2013.

Kaluza, T., Kunkel, D., and Hoor, P.: On the occurrence of strong vertical wind shear in the tropopause region: a 10-year ERA5 northern hemispheric study, Weather Clim. Dynam., 2, 631–651, https://doi.org/10.5194/wcd-2-631-2021, 2021.

Kedzierski, R. P., Neef, L., and Matthes, K.: Tropopause sharpening by data assimilation, Geophys. Res. Lett., 43, 8298–8305, https://doi.org/10.1002/2016gl069936, 2016.

Komhyr, W. D.: Operations handbook: Ozone measurements to 40 km altitude with model 4AECC-ozone sondes, NOAA Tech. Memo., eRLARL-149, 49 pp., https://repository.library.noaa.gov/view/noaa/22832 (last access: 1 February 2023), 1986.

Komhyr, W. D., Barnes, R. A., Brothers, G. B., Lathrop, J. A., and Opperman, D. P.: Electrochemical concentration cell ozonesonde performance evaluation during STOIC 1989, J. Geophys. Res., 100, 9231, https://doi.org/10.1029/94jd02175, 1995.

Krause, J., Hoor, P., Engel, A., Plöger, F., Grooß, J.-U., Bönisch, H., Keber, T., Sinnhuber, B.-M., Woiwode, W., and Oelhaf, H.: Mixing and ageing in the polar lower stratosphere in winter 2015–2016, Atmos. Chem. Phys., 18, 6057–6073, https://doi.org/10.5194/acp-18-6057-2018, 2018.

Kunkel, D., Hoor, P., Petropavlovskikh, I., and Manney, G. L.: Report on the first SPARC OCTAV-UTLS meeting, 18–20 July 2017, Boulder, USA, SPARC, https://www.sparc-climate.org/wp-content/uploads/sites/5/2018/02/SPARCnewsletterFeb2018_small-2.pdf (last access: 1 February 2023), 2018.

Kunkel, D., Hoor, P., Kaluza, T., Ungermann, J., Kluschat, B., Giez, A., Lachnitt, H.-C., Kaufmann, M., and Riese, M.: Evidence of small-scale quasi-isentropic mixing in ridges of extratropical baroclinic waves, Atmos. Chem. Phys., 19, 12607–12630, https://doi.org/10.5194/acp-19-12607-2019, 2019.

Kunz, A., Konopka, P., Müller, R., and Pan, L. L.: Dynamical tropopause based on isentropic potential vorticity gradients, J. Geophys. Res., 116, D01110, https://doi.org/10.1029/2010jd014343, 2011a.

Kunz, A., Pan, L. L., Konopka, P., Kinnison, D. E., and Tilmes, S.: Chemical and dynamical discontinuity at the extratropical tropopause based on START08 and WACCM analyses, J. Geophys. Res.-Atmos., 116, D24302, https://doi.org/10.1029/2011jd016686, 2011b.

Lait, L. R., Newman, P. A., Schoeberl, M. R., McGee, T., Twigg, L., Browell, E. V., Fenn, M. A., Grant, W. B., Butler, C. F., Bevilacqua, R., Davies, J., DeBacker, H., Andersen, S. B., Kyrö, E., Kivi, E., von der Gathen, P., Claude, H., Benesova, A., Skrivankova, P., Dorokhov, V., Zaitcev, I., Braathen, G., Gil, M., Litynska, Z., Moore, D., and Gerding, M.: Non-coincident interinstrument comparisons of ozone measurements using quasi-conservative coordinates, Atmos. Chem. Phys., 4, 2345–2352, https://doi.org/10.5194/acp-4-2345-2004, 2004.

Langford, A., Alvarez, R., Brioude, J., Evan, S., Iraci, L., Kirgis, G., Kuang, S., Leblanc, T., Newchurch, M., Pierce, R., Senff, C., and Yates, E.: Coordinated profiling of stratospheric intrusions and transported pollution by the Tropospheric Ozone Lidar Network (TOLNet) and NASA Alpha Jet experiment (AJAX): Observations and comparison to HYSPLIT, RAQMS, and FLEXPART, Atmos. Environ., 174, 1–14, https://doi.org/10.1016/j.atmosenv.2017.11.031, 2018.

Lawless, A. S.: A note on the analysis error associated with 3D-FGAT, Q. J. Roy. Meteor. Soc., 136, 1094–1098, https://doi.org/10.1002/qj.619, 2010.

Leblanc, T., McDermid, I. S., and Walsh, T. D.: Ground-based water vapor raman lidar measurements up to the upper troposphere and lower stratosphere for long-term monitoring, Atmos. Meas. Tech., 5, 17–36, https://doi.org/10.5194/amt-5-17-2012, 2012.

Leblanc, T., Sica, R. J., van Gijsel, J. A. E., Godin-Beekmann, S., Haefele, A., Trickl, T., Payen, G., and Liberti, G.: Proposed standardized definitions for vertical resolution and uncertainty in the NDACC lidar ozone and temperature algorithms – Part 2: Ozone DIAL uncertainty budget, Atmos. Meas. Tech., 9, 4051–4078, https://doi.org/10.5194/amt-9-4051-2016, 2016.

Leblanc, T., Brewer, M. A., Wang, P. S., Granados-Muñoz, M. J., Strawbridge, K. B., Travis, M., Firanski, B., Sullivan, J. T., McGee, T. J., Sumnicht, G. K., Twigg, L. W., Berkoff, T. A., Carrion, W., Gronoff, G., Aknan, A., Chen, G., Alvarez, R. J., Langford, A. O., Senff, C. J., Kirgis, G., Johnson, M. S., Kuang, S., and Newchurch, M. J.: Validation of the TOLNet lidars: the Southern California Ozone Observation Project (SCOOP), Atmos. Meas. Tech., 11, 6137–6162, https://doi.org/10.5194/amt-11-6137-2018, 2018.

Leblanc, T., Millán, L., Hoor, P., and Petropavlovskikh, I.: The third SPARC OCTAV-UTLS meeting, 3–5 March 2020, Wrightwood, CA, USA, SPARC, https://www.sparc-climate.org/wp-content/uploads/sites/5/2020/08/SPARCnewsletter_Jul2020_web20200806.pdf (last access: 1 February 2023), 2020.

Leovy, C., Sun, C.-R., Hitchman, M., Remsberg, E., Russell III, J., Gordley, L., Gille, J., and Lyjak, L.: Transport of Ozone in the Middle Stratosphere: Evidence for Planetary Wave Breaking, J. Atmos. Sci., 42, 230–244, https://doi.org/10.1175/1520-0469(1985)042<0230:TOOITM>2.0.CO;2, 1985.

Lin, M., Fiore, A. M., Horowitz, L. W., Langford, A. O., Oltmans, S. J., Tarasick, D., and Rieder, H. E.: Climate variability modulates western US ozone air quality in spring

via deep stratospheric intrusions, Nat. Commun., 6, 7105, https://doi.org/10.1038/ncomms8105, 2015.

Livesey, N. J., Filipiak, M. J., Froidevaux, L., Read, W. G., Lambert, A., Santee, M. L., Jiang, J. H., Pumphrey, H. C., Waters, J. W., Cofield, R. E., Cuddy, D. T., Daffer, W. H., Drouin, B. J., Fuller, R. A., Jarnot, R. F., Jiang, Y. B., Knosp, B. W., Li, Q. B., Perun, V. S., Schwartz, M. J., Snyder, W. V., Stek, P. C., Thurstans, R. P., Wagner, P. A., Avery, M., Browell, E. V., Cammas, J.-P., Christensen, L. E., Diskin, G. S., Gao, R.-S., Jost, H.-J., Loewenstein, M., Lopez, J. D., Nedelec, P., Osterman, G. B., Sachse, G. W., and Webster, C. R.: Validation of Aura Microwave Limb Sounder O_3 and CO observations in the upper troposphere and lower stratosphere, J. Geophys. Res.-Atmos., 113, D15S02, https://doi.org/10.1029/2007JD008805, 2008.

Livesey, N. J., Read, W., Wagner, P. A. Froidevaux, L., Lambert, A., Manney, G. L., Millán Valle, L., Pumphrey, H. C., Santee, M. L., Schwartz, M. J., Wang, S., Fuller, R. A., Jarnot, R. F., Knosp, B. W., and Martinez, E.: Version 4.2x Level 2 data quality and description document, Jet propulsion laboratory, JPL D-33509 Rev. E, http://mls.jpl.nasa.gov (last access: 1 February 2023), 2020.

Llewellyn, E. J., Lloyd, N. D., Degenstein, D. A., Gattinger, R. L., Petelina, S. V., Bourassa, A. E., Wiensz, J. T., Ivanov, E. V., McDade, I. C., Solheim, B. H., McConnell, J. C., Haley, C. S., von Savigny, C., Sioris, C. E., McLinden, C. A., Griffioen, E., Kaminski, J., Evans, W. F., Puckrin, E., Strong, K., Wehrle, V., Hum, R. H., Kendall, D. J., Matsushita, J., Murtagh, D. P., Brohede, S., Stegman, J., Witt, G., Barnes, G., Payne, W. F., Piché, L., Smith, K., Warshaw, G., Deslauniers, D. L., Marchand, P., Richardson, E. H., King, R. A., Wevers, I., McCreath, W., Kyrölä, E., Oikarinen, L., Leppelmeier, G. W., Auvinen, H., Mégie, G., Hauchecorne, A., Lefèvre, F., de La Nöe, J., Ricaud, P., Frisk, U., Sjoberg, F., von Schéele, F., and Nordh, L.: The OSIRIS instrument on the Odin spacecraft, Can. J. Phys., 82, 411–422, https://doi.org/10.1139/p04-005, 2004.

Long, C. S., Fujiwara, M., Davis, S., Mitchell, D. M., and Wright, C. J.: Climatology and interannual variability of dynamic variables in multiple reanalyses evaluated by the SPARC Reanalysis Intercomparison Project (S-RIP), Atmos. Chem. Phys., 17, 14593–14629, https://doi.org/10.5194/acp-17-14593-2017, 2017.

Lumpe, J., Bevilacqua, R., Randall, C., Nedoluha, G., Hoppel, K., Russell, J., Harvey, V. L., Schiller, C., Sen, B., Taha, G., Toon, G., and Vömel, H.: Validation of Polar Ozone and Aerosol Measurement (POAM) III version 4 stratospheric water vapor, J. Geophys. Res.-Atmos., 111, D11301, https://doi.org/10.1029/2005JD006763, 2006.

Lumpe, J. D., Fromm, M., Hoppel, K., Bevilacqua, R. M., Randall, C. E., Browell, E. V., Grant, W. B., McGee, T., Burris, J., Twigg, L., Richard, E. C., Toon, G. C., Margitan, J. J., Sen, B., Pfeilsticker, K., Boesch, H., Fitzenberger, R., Goutail, F., and Pommereau, J.-P.: Comparison of POAM III ozone measurements with correlative aircraft and balloon data during SOLVE, J. Geophys. Res.-Atmos., 107, 8316, https://doi.org/10.1029/2001JD000472, 2002.

Manney, G. L. and Hegglin, M. I.: Seasonal and Regional Variations of Long-Term Changes in Upper-Tropospheric Jets from Reanalyses, J. Climate, 31, 423–448, https://doi.org/10.1175/jcli-d-17-0303.1, 2018.

Manney, G. L., Harwood, R. S., MacKenzie, I. A., Minschwaner, K., Allen, D. R., Santee, M. L., Walker, K. A., Hegglin, M. I., Lambert, A., Pumphrey, H. C., Bernath, P. F., Boone, C. D., Schwartz, M. J., Livesey, N. J., Daffer, W. H., and Fuller, R. A.: Satellite observations and modeling of transport in the upper troposphere through the lower mesosphere during the 2006 major stratospheric sudden warming, Atmos. Chem. Phys., 9, 4775–4795, https://doi.org/10.5194/acp-9-4775-2009, 2009.

Manney, G. L., Hegglin, M. I., Daffer, W. H., Santee, M. L., Ray, E. A., Pawson, S., Schwartz, M. J., Boone, C. D., Froidevaux, L., Livesey, N. J., Read, W. G., and Walker, K. A.: Jet characterization in the upper troposphere/lower stratosphere (UTLS): applications to climatology and transport studies, Atmos. Chem. Phys., 11, 6115–6137, https://doi.org/10.5194/acp-11-6115-2011, 2011.

Manney, G. L., Hegglin, M., Daffer, W. H., Schwartz, M. J., Santee, M. L., and Pawson, S.: Climatology of Upper Tropospheric–Lower Stratospheric (UTLS) Jets and Tropopauses in MERRA, J. Climate, 27, 3248–3271, https://doi.org/10.1175/JCLI-D-13-00243.1, 2014.

Manney, G. L., Hegglin, M. I., Lawrence, Z. D., Wargan, K., Millán, L. F., Schwartz, M. J., Santee, M. L., Lambert, A., Pawson, S., Knosp, B. W., Fuller, R. A., and Daffer, W. H.: Reanalysis comparisons of upper tropospheric–lower stratospheric jets and multiple tropopauses, Atmos. Chem. Phys., 17, 11541–11566, https://doi.org/10.5194/acp-17-11541-2017, 2017.

Manney, G. L., Livesey, N. J., Santee, M. L., Froidevaux, L., Lambert, A., Lawrence, Z. D., Millán, L. F., Neu, J. L., Read, W. G., Schwartz, M. J., and Fuller, R. A.: Record-Low Arctic Stratospheric Ozone in 2020: MLS Observations of Chemical Processes and Comparisons With Previous Extreme Winters, Geophys. Res. Lett., 47, e2020GL089063, https://doi.org/10.1029/2020gl089063, 2020.

Manney, G. L., Hegglin, M. I., and Lawrence, Z. D.: Seasonal and Regional Signatures of ENSO in Upper Tropospheric Jet Characteristics from Reanalyses, J. Climate, 34, 9181–9200, https://doi.org/10.1175/JCLI-D-20-0947.1, 2021a.

Manney, G. L., Santee, M. L., Lawrence, Z. D., Wargan, K., and Schwartz, M. J.: A Moments View of Climatology and Variability of the Asian Summer Monsoon Anticyclone, J. Climate, 34, 7821–7841, https://doi.org/10.1175/jcli-d-20-0729.1, 2021b.

Martínez-Alonso, S., Deeter, M. N., Worden, H. M., Gille, J. C., Emmons, L. K., Pan, L. L., Park, M., Manney, G. L., Bernath, P. F., Boone, C. D., Walker, K. A., Kolonjari, F., Wofsy, S. C., Pittman, J., and Daube, B. C.: Comparison of upper tropospheric carbon monoxide from MOPITT, ACE-FTS, and HIPPO-QCLS, J. Geophys. Res.-Atmos., 119, 14144–14164, https://doi.org/10.1002/2014JD022397, 2014.

Match, A. and Gerber, E. P.: Tropospheric Expansion Under Global Warming Reduces Tropical Lower Stratospheric Ozone, Geophys. Res. Lett., 49, e2022GL099463, https://doi.org/10.1029/2022gl099463, 2022.

McCormick, M. P., Lei, L., Hill, M. T., Anderson, J., Querel, R., and Steinbrecht, W.: Early results and validation of SAGE III-ISS ozone profile measurements from onboard the International Space Station, Atmos. Meas. Tech., 13, 1287–1297, https://doi.org/10.5194/amt-13-1287-2020, 2020.

Mégie, G., Allain, J. Y., Chanin, M. L., and Blamont, J. E.: Vertical profile of stratospheric ozone by lidar sounding from the ground, Nature, 270, 329–331, https://doi.org/10.1038/270329a0, 1977.

Mettig, N., Weber, M., Rozanov, A., Burrows, J. P., Veefkind, P., Thompson, A. M., Stauffer, R. M., Leblanc, T., Ancellet, G., Newchurch, M. J., Kuang, S., Kivi, R., Tully, M. B., Van Malderen, R., Piters, A., Kois, B., Stübi, R., and Skrivankova, P.: Combined UV and IR ozone profile retrieval from TROPOMI and CrIS measurements, Atmos. Meas. Tech., 15, 2955–2978, https://doi.org/10.5194/amt-15-2955-2022, 2022.

Michelsen, H. A., Manney, G. L., Irion, F. W., Toon, G. C., Gunson, M. R., Rinsland, C. P., Zander, R., Mahieu, E., Newchurch, M. J., Purcell, P. N., Remsberg, E. E., Russell, J. M., Pumphrey, H. C., Waters, J. W., Bevilacqua, R. M., Kelly, K. K., Hintsa, E. J., Weinstock, E. M., Chiou, E.-W., Chu, W. P., McCormick, M. P., and Webster, C. R.: ATMOS version 3 water vapor measurements: Comparisons with observations from two ER-2 Lyman-α hygrometers, MkIV, HALOE, SAGE II, MAS, and MLS, J. Geophys. Res.-Atmos., 107, ACH 2-1–ACH 2-19, https://doi.org/10.1029/2001JD000587, 2002.

Millán, L. F. and Manney, G. L.: An assessment of ozone mini-hole representation in reanalyses over the Northern Hemisphere, Atmos. Chem. Phys., 17, 9277–9289, https://doi.org/10.5194/acp-17-9277-2017, 2017.

Millán, L. F., Livesey, N. J., Santee, M. L., Neu, J. L., Manney, G. L., and Fuller, R. A.: Case studies of the impact of orbital sampling on stratospheric trend detection and derivation of tropical vertical velocities: solar occultation vs. limb emission sounding, Atmos. Chem. Phys., 16, 11521–11534, https://doi.org/10.5194/acp-16-11521-2016, 2016.

Millán, L. F., Livesey, N. J., Santee, M. L., and von Clarmann, T.: Characterizing sampling and quality screening biases in infrared and microwave limb sounding, Atmos. Chem. Phys., 18, 4187–4199, https://doi.org/10.5194/acp-18-4187-2018, 2018.

Millán, L. F., Manney, G. L., and Lawrence, Z. D.: Reanalysis intercomparison of potential vorticity and potential-vorticity-based diagnostics, Atmos. Chem. Phys., 21, 5355–5376, https://doi.org/10.5194/acp-21-5355-2021, 2021.

Miyazaki, K. and Bowman, K.: Evaluation of ACCMIP ozone simulations and ozonesonde sampling biases using a satellite-based multi-constituent chemical reanalysis, Atmos. Chem. Phys., 17, 8285–8312, https://doi.org/10.5194/acp-17-8285-2017, 2017.

Monahan, K. P., Pan, L. L., McDonald, A. J., Bodeker, G. E., Wei, J., George, S. E., Barnet, C. D., and Maddy, E.: Validation of AIRS v4 ozone profiles in the UTLS using ozonesondes from Lauder, NZ and Boulder, USA, J. Geophys. Res.-Atmos., 112, D17304, https://doi.org/10.1029/2006JD008181, 2007.

Morgan, M. C. and Nielsen-Gammon, J. W.: Using Tropopause Maps to Diagnose Midlatitude Weather Systems, Mon. Weather Rev., 126, 2555–2579, https://doi.org/10.1175/1520-0493(1998)126<2555:utmtdm>2.0.co;2, 1998.

Müller, S., Hoor, P., Bozem, H., Gute, E., Vogel, B., Zahn, A., Bönisch, H., Keber, T., Krämer, M., Rolf, C., Riese, M., Schlager, H., and Engel, A.: Impact of the Asian monsoon on the extratropical lower stratosphere: trace gas observations during TACTS over Europe 2012, Atmos. Chem. Phys., 16, 10573–10589, https://doi.org/10.5194/acp-16-10573-2016, 2016.

Network for the Detection of Atmospheric Composition Change: Lidar, NASA [data set], https://www-air.larc.nasa.gov/missions/ndacc/data.html, last access: 1 February 2023.

Oelhaf, H., Sinnhuber, B.-M., Woiwode, W., Bönisch, H., Bozem, H., Engel, A., Fix, A., Friedl-Vallon, F., Grooß, J.-U., Hoor, P., Johansson, S., Jurkat-Witschas, T., Kaufmann, S., Krämer, M., Krause, J., Kretschmer, E., Lörks, D., Marsing, A., Orphal, J., Pfeilsticker, K., Pitts, M., Poole, L., Preusse, P., Rapp, M., Riese, M., Rolf, C., Ungermann, J., Voigt, C., Volk, C. M., Wirth, M., Zahn, A., and Ziereis, H.: POLSTRACC: Airborne Experiment for Studying the Polar Stratosphere in a Changing Climate with the High Altitude and Long Range Research Aircraft (HALO), B. Am. Meteorol. Soc., 100, 2634–2664, https://doi.org/10.1175/bams-d-18-0181.1, 2019.

Olsen, M. A., Manney, G. L., and Liu, J.: The ENSO and QBO Impact on Ozone Variability and Stratosphere-Troposphere Exchange Relative to the Subtropical Jets, J. Geophys. Res.-Atmos., 124, 7379–7392, https://doi.org/10.1029/2019jd030435, 2019.

Orbe, C., Wargan, K., Pawson, S., and Oman, L. D.: Mechanisms Linked to Recent Ozone Decreases in the Northern Hemisphere Lower Stratosphere, J. Geophys. Res.-Atmos., 125, e2019JD031631, https://doi.org/10.1029/2019jd031631, 2020.

Pan, L. L., Randel, W. J., Gary, B. L., Mahoney, M. J., and Hintsa, E. J.: Definitions and sharpness of the extratropical tropopause: A trace gas perspective, J. Geophys. Res.-Atmos., 109, D23103, https://doi.org/10.1029/2004JD004982, 2004.

Pan, L. L., Randel, W. J., Gille, J. C., Hall, W. D., Nardi, B., Massie, S., Yudin, V., Khosravi, R., Konopka, P., and Tarasick, D.: Tropospheric intrusions associated with the secondary tropopause, J. Geophys. Res., 114, D10302, https://doi.org/10.1029/2008jd011374, 2009.

Pan, L. L., Bowman, K. P., Atlas, E. P., Wofsy, S. C., Zhang, F., Bresch, J. F., Ridley, B. A., Pittman, J. V., Homeyer, C. P., Romashkin, P., and Cooper, W. A.: The Stratosphere-Troposphere Analysis of Regional Transport 2008 Experiment, B. Am. Meteorol. Soc., 91, 327–342, 2010.

Pan, L. L., Kunz, A., Homeyer, C. R., Munchak, L. A., Kinnison, D. E., and Tilmes, S.: Commentary on using equivalent latitude in the upper troposphere and lower stratosphere, Atmos. Chem. Phys., 12, 9187–9199, https://doi.org/10.5194/acp-12-9187-2012, 2012.

Peevey, T. R., Gille, J. C., Homeyer, C. R., and Manney, G. L.: The double tropopause and its dynamical relationship to the tropopause inversion layer in storm track regions, J. Geophys. Res., 119, 10194–10212, https://doi.org/10.1002/2014JD021808, 2014.

Petropavlovskikh, I., Godin-Beekmann, S., Hubert, D., Damadeo, R., Hassler, B., and Sofieva, V.: SPARC/IO3C/GAW Report on Long-term Ozone Trends and Uncertainties in the Stratosphere, SPARC, https://doi.org/10.17874/F899E57A20B, 2019.

Petzold, A., Thouret, V., Gerbig, C., Zahn, A., Brenninkmeijer, C. A. M., Gallagher, M., Hermann, M., Pontaud, M., Ziereis, H., Boulanger, D., Marshall, J., Nédélec, P., Smit, H. G. J., Friess, U., Flaud, J.-M., Wahner, A., Cammas, J.-P., Volz-Thomas, A., and Team, I.: Global-scale atmosphere monitoring by in-service aircraft – current achievements and future prospects of the European Research Infrastructure IAGOS, Tellus B, 67, 28452, https://doi.org/10.3402/tellusb.v67.28452, 2015.

Pittman, J. V., Pan, L. L., Wei, J. C., Irion, F. W., Liu, X., Maddy, E. S., Barnet, C. D., Chance, K., and Gao, R.-S.: Evaluation of AIRS, IASI, and OMI ozone profile retrievals in the extratropical tropopause region using in situ aircraft measurements, J. Geophys. Res.-Atmos., 114, D24109, https://doi.org/10.1029/2009JD012493, 2009.

Randel, W. J., Seidel, D. J., and Pan, L. L.: Observational characteristics of double tropopauses, J. Geophys. Res.-Atmos., 112, D07309, https://doi.org/10.1029/2006JD007904, 2007.

Ravetta, F., Ancellet, G., Colette, A., and Schlager, H.: Long-range transport and tropospheric ozone variability in the western Mediterranean region during the Intercontinental Transport of Ozone and Precursors (ITOP-2004) campaign, J. Geophys. Res.-Atmos., 112, D10S46, https://doi.org/10.1029/2006jd007724, 2007.

Riese, M., Ploeger, F., Rap, A., Vogel, B., Konopka, P., Dameris, M., and Forster, P.: Impact of uncertainties in atmospheric mixing on simulated UTLS composition and related radiative effects, J. Geophys. Res.-Atmos., 117, D16305, https://doi.org/10.1029/2012jd017751, 2012.

Ryan, N. J., Palm, M., Raffalski, U., Larsson, R., Manney, G., Millán, L., and Notholt, J.: Strato-mesospheric carbon monoxide profiles above Kiruna, Sweden (67.8° N, 20.4° E), since 2008, Earth Syst. Sci. Data, 9, 77–89, https://doi.org/10.5194/essd-9-77-2017, 2017.

Santee, M. L., Manney, G. L., Livesey, N. J., Schwartz, M. J., Neu, J. L., and Read, W. G.: A comprehensive overview of the climatological composition of the Asian summer monsoon anticyclone based on 10 years of Aura Microwave Limb Sounder measurements, J. Geophys. Res.-Atmos., 122, 5491–5514, https://doi.org/10.1002/2016jd026408, 2017.

Schoeberl, M. R.: Extratropical stratosphere-troposphere mass exchange, J. Geophys. Res.-Atmos., 109, D13303, https://doi.org/10.1029/2004JD004525, 2004.

Schoeberl, M. R., Luo, M., and Rosenfield, J. E.: An analysis of the Antarctic Halogen Occultation Experiment trace gas observations, J. Geophys. Res.-Atmos., 100, 5159–5172, https://doi.org/10.1029/94JD02749, 1995.

Schwartz, M., Froidevaux, L., Livesey, N., and Read, W.: MLS/Aura Level 2 Ozone (O_3) Mixing Ratio V005, Greenbelt, MD, USA, Goddard Earth Sciences Data and Information Services Center (GES DISC) [data set], https://doi.org/10.5067/Aura/MLS/DATA2516, 2020.

Schwartz, M. J., Manney, G. L., Hegglin, M. I., Livesey, N. J., Santee, M. L., and Daffer, W. H.: Climatology and variability of trace gases in extratropical double-tropopause regions from MLS, HIRDLS, and ACE-FTS measurements, J. Geophys. Res.-Atmos., 120, 843–867, https://doi.org/10.1002/2014jd021964, 2015.

Seftor, C. J., Jaross, G., Kowitt, M., Haken, M., Li, J., and Flynn, L. E.: Postlaunch performance of the Suomi National Polar-orbiting Partnership Ozone Mapping and Profiler Suite (OMPS) nadir sensors, J. Geophys. Res.-Atmos., 119, 4413–4428, https://doi.org/10.1002/2013jd020472, 2014.

Sheese, P. and Walker, K.: Data Quality Flags for ACE-FTS Level 2 Version 4.1/4.2 Data Set, Borealis, V28 [data set], https://doi.org/10.5683/SP2/BC4ATC, 2020.

Sheese, P. E., Walker, K. A., Boone, C. D., Bernath, P. F., Froidevaux, L., Funke, B., Raspollini, P., and von Clarmann, T.: ACE-FTS ozone, water vapour, nitrous oxide, nitric acid, and carbon monoxide profile comparisons with MIPAS and MLS, J. Quant. Spectrosc. Ra., 186, 63–80, https://doi.org/10.1016/j.jqsrt.2016.06.026, 2017.

Sheese, P. E., Walker, K. A., Boone, C. D., Bourassa, A. E., Degenstein, D. A., Froidevaux, L., McElroy, C. T., Murtagh, D., Russell III, J. M., and Zou, J.: Assessment of the quality of ACE-FTS stratospheric ozone data, Atmos. Meas. Tech., 15, 1233–1249, https://doi.org/10.5194/amt-15-1233-2022, 2022.

Smit, H. G. J., Straeter, W., Johnson, B. J., Oltmans, S. J., Davies, J., Tarasick, D. W., Hoegger, B., Stubi, R., Schmidlin, F. J., Northam, T., Thompson, A. M., Witte, J. C., Boyd, I., and Posny, F.: Assessment of the performance of ECC-ozonesondes under quasi-flight conditions in the environmental simulation chamber: Insights from the Juelich Ozone Sonde Intercomparison Experiment (JOSIE), J. Geophys. Res., 112, D19306, https://doi.org/10.1029/2006jd007308, 2007.

Spensberger, C. and Spengler, T.: Feature-Based Jet Variability in the Upper Troposphere, J. Climate, 33, 6849–6871, https://doi.org/10.1175/jcli-d-19-0715.1, 2020.

Steinbrecht, W., Claude, H., Schönenborn, F., McDermid, I. S., Leblanc, T., Godin-Beekmann, S., Keckhut, P., Hauchecorne, A., Gijsel, J. A. E. V., Swart, D. P. J., Bodeker, G. E., Parrish, A., Boyd, I. S., Kämpfer, N., Hocke, K., Stolarski, R. S., Frith, S. M., Thomason, L. W., Remsberg, E. E., Savigny, C. V., Rozanov, A., and Burrows, J. P.: Ozone and temperature trends in the upper stratosphere at five stations of the Network for the Detection of Atmospheric Composition Change, Int. J. Remote Sens., 30, 3875–3886, https://doi.org/10.1080/01431160902821841, 2009.

Steinbrecht, W., Froidevaux, L., Fuller, R., Wang, R., Anderson, J., Roth, C., Bourassa, A., Degenstein, D., Damadeo, R., Zawodny, J., Frith, S., McPeters, R., Bhartia, P., Wild, J., Long, C., Davis, S., Rosenlof, K., Sofieva, V., Walker, K., Rahpoe, N., Rozanov, A., Weber, M., Laeng, A., von Clarmann, T., Stiller, G., Kramarova, N., Godin-Beekmann, S., Leblanc, T., Querel, R., Swart, D., Boyd, I., Hocke, K., Kämpfer, N., Maillard Barras, E., Moreira, L., Nedoluha, G., Vigouroux, C., Blumenstock, T., Schneider, M., García, O., Jones, N., Mahieu, E., Smale, D., Kotkamp, M., Robinson, J., Petropavlovskikh, I., Harris, N., Hassler, B., Hubert, D., and Tummon, F.: An update on ozone profile trends for the period 2000 to 2016, Atmos. Chem. Phys., 17, 10675–10690, https://doi.org/10.5194/acp-17-10675-2017, 2017.

Sterling, C. W., Johnson, B. J., Oltmans, S. J., Smit, H. G. J., Jordan, A. F., Cullis, P. D., Hall, E. G., Thompson, A. M., and Witte, J. C.: Homogenizing and estimating the uncertainty in NOAA's long-term vertical ozone profile records measured with the electrochemical concentration cell ozonesonde, Atmos. Meas. Tech., 11, 3661–3687, https://doi.org/10.5194/amt-11-3661-2018, 2018.

Stone, K. A., Solomon, S., and Kinnison, D. E.: On the Identification of Ozone Recovery, Geophys. Res. Lett., 45, 5158–5165, https://doi.org/10.1029/2018gl077955, 2018.

Strahan, S. E.: Climatologies of lower stratospheric NO_y and O_3 and correlations with N_2O based on in situ observations, J. Geophys. Res.-Atmos., 104, 30463–30480, https://doi.org/10.1029/1999jd900775, 1999.

Strong, C. and Davis, R. E.: Variability in the Position and Strength of Winter Jet Stream Cores Related to Northern Hemisphere Teleconnections, J. Climate, 21, 584–592, https://doi.org/10.1175/2007jcli1723.1, 2008.

Szeląg, M. E., Sofieva, V. F., Degenstein, D., Roth, C., Davis, S., and Froidevaux, L.: Seasonal stratospheric ozone trends over 2000–2018 derived from several merged data sets, Atmos. Chem. Phys., 20, 7035–7047, https://doi.org/10.5194/acp-20-7035-2020, 2020.

Tarasick, D. W., Smit, H. G. J., Thompson, A. M., Morris, G. A., Witte, J. C., Davies, J., Nakano, T., Malderen, R. V., Stauffer, R. M., Johnson, B. J., Stübi, R., Oltmans, S. J., and Vömel, H.: Improving ECC Ozonesonde Data Quality: Assessment of Current Methods and Outstanding Issues, Earth Space Sci., 8, e2019EA000914, https://doi.org/10.1029/2019ea000914, 2021.

Tegtmeier, S., Krüger, K., Birner, T., Davis, N. A., Davis, S., Fujiwara, M., Homeyer, C. R., Ivanciu, I., Kim, Y.-H., Legras, B., Manney, G. L., Nishimoto, E., Nützel, M., Pilch Kedzierski, R., Wang, J. S., Wang, T., and Wright, J. S.: Tropical Troposphere Layer, in: S-RIP Final Report, edited by: Fujiwara, M., Manney, G. L., Grey, L. J., and Wright, J. S., chap. 8, SPARC, https://www.sparc-climate.org/wp-content/uploads/sites/5/2022/04/08_S-RIP_Report_Ch08.pdf (last access: 1 February 2023), 2022.

Tereszchuk, K. A., González Abad, G., Clerbaux, C., Hurtmans, D., Coheur, P.-F., and Bernath, P. F.: ACE-FTS measurements of trace species in the characterization of biomass burning plumes, Atmos. Chem. Phys., 11, 12169–12179, https://doi.org/10.5194/acp-11-12169-2011, 2011.

Tereszchuk, K. A., González Abad, G., Clerbaux, C., Hadji-Lazaro, J., Hurtmans, D., Coheur, P.-F., and Bernath, P. F.: ACE-FTS observations of pyrogenic trace species in boreal biomass burning plumes during BORTAS, Atmos. Chem. Phys., 13, 4529–4541, https://doi.org/10.5194/acp-13-4529-2013, 2013.

Thomason, L. W., Ernest, N., Millán, L., Rieger, L., Bourassa, A., Vernier, J.-P., Manney, G., Luo, B., Arfeuille, F., and Peter, T.: A global space-based stratospheric aerosol climatology: 1979–2016, Earth Syst. Sci. Data, 10, 469–492, https://doi.org/10.5194/essd-10-469-2018, 2018.

Thompson, A. M., Witte, J. C., Sterling, C., Jordan, A., Johnson, B. J., Oltmans, S. J., Fujiwara, M., Vömel, H., Allaart, M., Piters, A., Coetzee, G. J. R., Posny, F., Corrales, E., Diaz, J. A., Félix, C., Komala, N., Lai, N., Nguyen, H. T. A., Maata, M., Mani, F., Zainal, Z., ya Ogino, S., Paredes, F., Penha, T. L. B., Silva, F. R., Sallons-Mitro, S., Selkirk, H. B., Schmidlin, F. J., Stübi, R., and Thiongo, K.: First Reprocessing of Southern Hemisphere Additional Ozonesondes (SHADOZ) Ozone Profiles (1998–2016): 2. Comparisons With Satellites and Ground-Based Instruments, J. Geophys. Res.-Atmos., 122, 13000–13025, https://doi.org/10.1002/2017jd027406, 2017.

Thompson, A. M., Stauffer, R. M., Wargan, K., Witte, J. C., Kollonige, D. E., and Ziemke, J. R.: Regional and Seasonal Trends in Tropical Ozone From SHADOZ Profiles: Reference for Models and Satellite Products, J. Geophys. Res.-Atmos., 126, e2021JD034691, https://doi.org/10.1029/2021jd034691, 2021.

Thouret, V., Cammas, J.-P., Sauvage, B., Athier, G., Zbinden, R., Nédélec, P., Simon, P., and Karcher, F.: Tropopause referenced ozone climatology and inter-annual variability (1994–2003) from the MOZAIC programme, Atmos. Chem. Phys., 6, 1033–1051, https://doi.org/10.5194/acp-6-1033-2006, 2006.

Toohey, M., Hegglin, M. I., Tegtmeier, S., Anderson, J., Añel, J. A., Bourassa, A., Brohede, S., Degenstein, D., Froidevaux, L., Fuller, R., Funke, B., Gille, J., Jones, A., Kasai, Y., Krüger, K., Kyrölä, E., Neu, J. L., Rozanov, A., Smith, L., Urban, J., von Clarmann, T., Walker, K. A., and Wang, R. H. J.: Characterizing sampling biases in the trace gas climatologies of the SPARC Data Initiative, J. Geophys. Res.-Atmos., 118, 11847–11862, https://doi.org/10.1002/jgrd.50874, 2013.

UCAR/NCAR: START08, NO-NOy-O3, Version 1.0, UCAR/NCAR – Earth Observing Laboratory [data set], https://doi.org/10.5065/D62V2DG5, 2011.

University of Waterloo: ACE-FTS, University of Waterloo [data set], http://www.ace.uwaterloo.ca/data.php, last access: 1 February 2023.

Velazco, V. A., Toon, G. C., Blavier, J.-F. L., Kleinböhl, A., Manney, G. L., Daffer, W. H., Bernath, P. F., Walker, K. A., and Boone, C.: Validation of the Atmospheric Chemistry Experiment by noncoincident MkIV balloon profiles, J. Geophys. Res., 116, D06306, https://doi.org/10.1029/2010jd014928, 2011.

Wang, H. J. R., Damadeo, R., Flittner, D., Kramarova, N., Taha, G., Davis, S., Thompson, A. M., Strahan, S., Wang, Y., Froidevaux, L., Degenstein, D., Bourassa, A., Steinbrecht, W., Walker, K. A., Querel, R., Leblanc, T., Godin-Beekmann, S., Hurst, D., and Hall, E.: Validation of SAGE III/ISS Solar Occultation Ozone Products With Correlative Satellite and Ground-Based Measurements, J. Geophys. Res.-Atmos., 125, e2020JD032430, https://doi.org/10.1029/2020jd032430, 2020.

Wargan, K. and Coy, L.: Strengthening of the Tropopause Inversion Layer during the 2009 Sudden Stratospheric Warming: A MERRA-2 Study, J. Atmos. Sci., 73, 1871–1887, https://doi.org/10.1175/jas-d-15-0333.1, 2016.

Wargan, K., Labow, G., Frith, S., Pawson, S., Livesey, N., and Partyka, G.: Evaluation of the Ozone Fields in NASA's MERRA-2 Reanalysis, J. Climate, 30, 2961–2988, https://doi.org/10.1175/jcli-d-16-0699.1, 2017.

Wargan, K., Orbe, C., Pawson, S., Ziemke, J. R., Oman, L. D., Olsen, M. A., Coy, L., and Knowland, K. E.: Recent Decline in Extratropical Lower Stratospheric Ozone Attributed to Circulation Changes, Geophys. Res. Lett., 45, 5166–5176, https://doi.org/10.1029/2018gl077406, 2018.

Waters, J. W., Froidevaux, L., Harwood, R. S., Jarnot, R. F., Pickett, H. M., Read, W. G., Siegel, P. H., Cofield, R. E., Filipiak, M. J., Flower, D. A., Holden, J. R., Lau, G. K., Livesey, N. J., Manney, G. L., Pumphrey, H. C., Santee, M. L., Wu, D. L., Cuddy, D. T., Lay, R. R., Loo, M. S., Perun, V. S., Schwartz, M. J., Stek, P. C., Thurstans, R. P., Boyles, M. A., Chandra, K. M., Chavez, M. C., Chen, G.-S., Chudasama, B. V., Dodge, R., Fuller, R. A., Girard, M. A., Jiang, J. H., Jiang, Y., Knosp, B. W., LaBelle, R. C., Lam, J. C., Lee, K. A., Miller, D., Oswald, J. E., Patel, N. C., Pukala, D. M., Quintero, O., Scaff, D. M., Snyder, W. V., Tope, M. C., Wagner, P. A., and Walch, M. J.: The Earth observing system microwave limb sounder (EOS MLS) on the aura Satellite, IEEE T. Geosci. Remote, 44, 1075–1092, https://doi.org/10.1109/TGRS.2006.873771, 2006.

Wing, R., Steinbrecht, W., Godin-Beekmann, S., McGee, T. J., Sullivan, J. T., Sumnicht, G., Ancellet, G., Hauchecorne, A., Khaykin, S., and Keckhut, P.: Intercomparison and evaluation of ground- and satellite-based stratospheric ozone and temperature profiles above Observatoire de Haute-Provence during the Lidar Validation NDACC Experiment (LAVANDE), Atmos. Meas. Tech., 13, 5621–5642, https://doi.org/10.5194/amt-13-5621-2020, 2020.

Witte, J. C., Thompson, A. M., Smit, H. G. J., Fujiwara, M., Posny, F., Coetzee, G. J. R., Northam, E. T., Johnson, B. J., Sterling, C. W., Mohamad, M., Ogino, S.-Y., Jordan, A., and da Silva, F. R.: First reprocessing of Southern Hemisphere ADditional OZonesondes (SHADOZ) profile records (1998–2015):

1. Methodology and evaluation, J. Geophys. Res.-Atmos., 122, 6611–6636, https://doi.org/10.1002/2016jd026403, 2017.

WMO: World Meteorological Organization (WMO), Meteorology A Three-Dimensional Science: Second Session of the Commission for Aerology WMO Bulletin IV(4), WMO, Geneva, 134–138, https://library.wmo.int/doc_num.php?explnum_id=6960 (last access: 1 February 2023), 1957.

Xian, T. and Homeyer, C. R.: Global tropopause altitudes in radiosondes and reanalyses, Atmos. Chem. Phys., 19, 5661–5678, https://doi.org/10.5194/acp-19-5661-2019, 2019.

Zahn, A., Weppner, J., Widmann, H., Schlote-Holubek, K., Burger, B., Kühner, T., and Franke, H.: A fast and precise chemiluminescence ozone detector for eddy flux and airborne application, Atmos. Meas. Tech., 5, 363–375, https://doi.org/10.5194/amt-5-363-2012, 2012.

Zerefos, C., Kapsomenakis, J., Eleftheratos, K., Tourpali, K., Petropavlovskikh, I., Hubert, D., Godin-Beekmann, S., Steinbrecht, W., Frith, S., Sofieva, V., and Hassler, B.: Representativeness of single lidar stations for zonally averaged ozone profiles, their trends and attribution to proxies, Atmos. Chem. Phys., 18, 6427–6440, https://doi.org/10.5194/acp-18-6427-2018, 2018.

Zhao, X., Weaver, D., Bognar, K., Manney, G., Millán, L., Yang, X., Eloranta, E., Schneider, M., and Strong, K.: Cyclone-induced surface ozone and HDO depletion in the Arctic, Atmos. Chem. Phys., 17, 14955–14974, https://doi.org/10.5194/acp-17-14955-2017, 2017.